

# Measurement of polarization observables of the associated strangeness production in proton proton interactions

The COSY-TOF Collaboration

F. Hauenstein<sup>1,4</sup>, E. Borodina<sup>1</sup>, H. Clement<sup>5,6</sup>, E. Doroshkevich<sup>5,6a</sup>, R. Dzhygadlo<sup>1b</sup>, K. Ehrhardt<sup>5,6</sup>, W. Eyrich<sup>4</sup>, W. Gast<sup>1</sup>, A. Gillitzer<sup>1</sup>, D. Grzonka<sup>1</sup>, S. Jowzaee<sup>1,7</sup>, P. Klaja<sup>1,4</sup>, L. Kober<sup>4</sup>, K. Kilian<sup>1</sup>, M. Krapp<sup>4</sup>, M. Mertens<sup>1c</sup>, P. Moskal<sup>7</sup>, J. Ritman<sup>1,2,8</sup>, E. Roderburg<sup>1d</sup>, M. Röder<sup>1e</sup>, W. Schroeder<sup>9</sup>, T. Sefzick<sup>1</sup>, J. Smyrski<sup>7</sup>, P. Wintz<sup>1</sup>, and P. Wüstner<sup>3</sup>

<sup>1</sup> Institut für Kernphysik, Forschungszentrum Jülich, 52428 Jülich, Germany

<sup>2</sup> Jülich Aachen Research Alliance, Forces and Matter Experiments (JARA-FAME)

<sup>3</sup> Zentralinstitut für Engineering, Elektronik und Analytik, 52428 Jülich, Germany

<sup>4</sup> Friedrich-Alexander-Universität Erlangen-Nürnberg, 91058 Erlangen, Germany

<sup>5</sup> Physikalisches Institut der Universität Tübingen, Auf der Morgenstelle 14, 72076 Tübingen, Germany

<sup>6</sup> Kepler Center for Astro and Particle Physics, University of Tübingen, Auf der Morgenstelle 14, 72076 Tübingen, Germany

<sup>7</sup> Institute of Physics, Jagellonian University, PL-30-348 Cracow, Poland

<sup>8</sup> Experimentalphysik I, Ruhr-Universität Bochum, 44780 Bochum, Germany

<sup>9</sup> Corporate Development, Forschungszentrum Jülich, 52428 Jülich, Germany

March 10, 2019

**Abstract.** The  $\Lambda$  polarization, the analyzing power, and the  $\Lambda$  spin transfer coefficient of the reaction  $pp \rightarrow pK^+\Lambda$  were measured at beam momenta of 2.70 GeV/c and 2.95 GeV/c, corresponding to excess energies of 122 MeV and 204 MeV. While the analyzing power and the spin transfer coefficient do not change significantly with the excess energy, the  $\Lambda$  polarization varies strongly and changes its sign. As this is the first measurement of polarization observables below an excess energy of 200 MeV, the change of the sign of the  $\Lambda$  polarization was not observed before. The high statistics of the data ( $\approx 200$  k events for each momentum) enables detailed studies of the dependence of the  $\Lambda$  polarization and the analyzing power on the center of mass momentum of the particles. The results of the spin transfer coefficient are in agreement with data from the DISTO experiment. No obvious agreement of the  $\Lambda$  polarization can be found in comparison with data of high momentum measurements.

## 1 Introduction

In this paper the results concerning the polarization observables of recent COSY-TOF measurements of  $pp \rightarrow pK^+\Lambda$  are presented. Angular distributions, Dalitz plots and invariant masses obtained from the 2.95 GeV/c measurement were discussed in a previous paper [1]. As polarization variables the  $\Lambda$  polarization, the analyzing power measured with the final state particles, and the  $\Lambda$  spin transfer coefficient are denoted. Due to the nearly  $4\pi$  acceptance of the COSY-TOF detector for this reaction it

is possible to measure the polarization observables for the whole kinematic range. The measurements of the analyzing power and the spin transfer coefficient require the polarization of the proton beam. This was provided from the COSY accelerator as an external beam with polarization degrees as high as 80–90%.

Since the first observation that  $\Lambda$ 's exhibit a polarization, even when produced with an unpolarized beam [2], many experiments had examined the dependence of this polarization on different kinematic variables. These experiments were performed with high beam momenta. No consistent behavior of the  $\Lambda$  polarization emerged from these measurements. Therefore, it is nearly impossible to determine parameters for model calculations [3]. Closer to threshold only inclusive data from HADES ( $p_{\text{beam}} = 4.34$  GeV/c) [4] and exclusive data from DISTO ( $p_{\text{beam}} = 3.67$  GeV/c) [5] exist. The COSY-TOF data discussed in this paper are the first ones, which give information of the  $\Lambda$  polarization as close as  $\epsilon = 122$  MeV above threshold.

<sup>a</sup> current address: Institute for Nuclear Research Moscow 117312, Russia

<sup>b</sup> current address: Hadron Physics I, GSI Helmholtzzentrum für Schwerionenforschung GmbH

<sup>c</sup> current address: Universität Duisburg-Essen 45141 Essen, Germany

<sup>d</sup> corresponding author e.roderburg@fz-juelich.de

<sup>e</sup> current address: Corporate Development, Forschungszentrum Jülich, 52428 Jülich, Germany

They exhibit a strong dependence of the  $\Lambda$  polarization on the excess energy, which was not observed before.

The analyzing power measured with the final state particles provides information on the involved angular momenta in the process in addition to the information that can be gained from the angular distributions. The measured distributions should help to determine parameters of a partial wave analysis, which is in preparation [6]. As most of the previous measurements were inclusive and high acceptance is needed for measurements of the analyzing power, the existing data are very scarce and partly still preliminary. As the COSY-TOF data cover the full accessible phase space, they can be described with Legendre polynomials and the dependence of the Legendre coefficients on the particle momenta is examined.

The measurement of the spin transfer coefficient combines information on the  $\Lambda$  polarization with the analyzing power by an event to event analysis. Apart from three measurements at high momenta, which were restricted in the kinematic range [7,8,9], the only exclusive measurements were published by the DISTO experiment [10]. The COSY-TOF data allow for the first time a comparison of this observable between independent measurements.

## 2 Experimental setup and analysis

The data were taken with the COSY-TOF spectrometer, which was situated at an external beam of the accelerator COSY/Jülich. The COSY-TOF detector is a non mag-

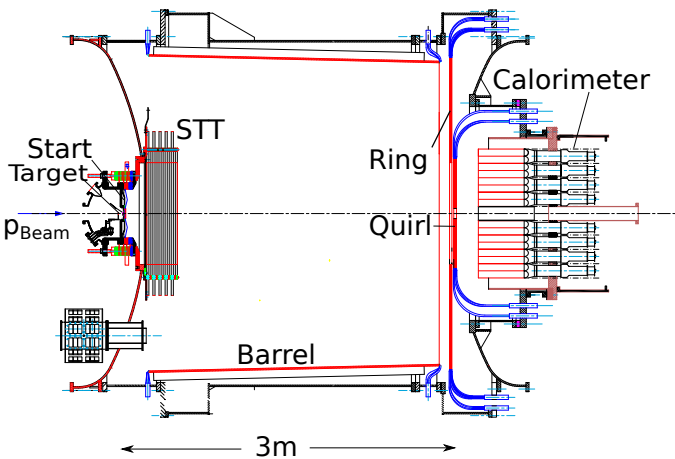


**Fig. 1.** Side view of the COSY-TOF spectrometer. In beam direction the start counter (Start), the straw tube tracker (STT) the barrel scintillators, the inner ring (Quirl), the outer ring (Ring) and the Calorimeter are shown. All detectors and the liquid hydrogen target are located inside the vacuum vessel.

netic spectrometer built as a cylindrical vacuum vessel, with 3.5m length and 3m diameter (see fig.1). The inner walls are covered with segmented scintillation counters, which define the trigger. The main components are the miniaturized liquid hydrogen target in cylinder form

with 6 mm diameter and 4 mm length and the straw tube tracker, from which precise information of the vertices and track directions are obtained. The detector is described in detail in [1].

The analysis of the  $pK^+\Lambda$  final state examines events, which are triggered by four or more hits in the scintillator hodoscopes. These events are fitted by a two vertices hypothesis: a primary vertex of  $pK^+$  and a secondary of the  $\Lambda$  decay. Events, for which this fit converges, are submitted to a kinematic fit procedure, which applies momentum and energy conservation and the masses of the involved particles. The assignment of the proton and kaon masses to the primary tracks is done by applying the kinematic fit for each possibility, the result with the lowest  $\chi^2$  is chosen [11,12].

The background introduced by multi-pion events is determined to be less than 5% by comparing the measured  $\Lambda$  decay length distribution to the expected distribution [1]. Special care has to be taken for the admixture of  $\Lambda$ 's from  $pp \rightarrow pK(\Sigma^0 \rightarrow \gamma\Lambda)$ , which dilutes the measured  $\Lambda$  polarization and introduces unknown errors to the spin transfer coefficient and to the analyzing power. The suppression of the  $\Sigma^0$  events by the  $\chi^2$  threshold for the kinematic fit is studied with a Monte Carlo sample of  $pK(\Sigma^0 \rightarrow \gamma\Lambda)$  events. Including the cross section ratios, the contamination of  $\Sigma^0$  events is less than 5% for the 2.95 GeV/c data [1] and less than 1% for the 2.70 GeV/c data [11]. From the Monte Carlo simulations it is known that the  $pp \rightarrow pK(\Sigma^0 \rightarrow \gamma\Lambda)$  events, are shifted by the kinematic fit, which assumes a  $pp \rightarrow pK\Lambda$  reaction, to backward kaon directions. Therefore, the 2.95 GeV/c data are analyzed in addition with a selection on the kaon angle of  $|\cos\theta_K^{\text{cm}}| < 0.9$  and compared with the results without this restriction. Apart from statistical fluctuations, no deviations are found in the distributions of all polarization observables.

In order to determine the beam polarization, a sample of elastic scattering events is recorded by a trigger, which demands at least two charged tracks. With cuts on the coplanarity and on the missing energy elastic scattered events are determined with a background of less than 1% [11]. By evaluating the left-right asymmetry of the elastic scattered protons and by comparing this distribution with the analyzing power determined with the partial wave analysis SAID [13] the averaged transverse beam polarization is determined. For the 2.70 GeV/c data it is  $(79.0 \pm 1.1)\%$  [11]. The 2.95 GeV/c data were acquired in two different runs, the first with 54,000 events had a polarization of  $(61.0 \pm 1.7)\%$  [14] and the second with 121,000 events had a polarization of  $(87.5 \pm 2.0)\%$  [12]. Both runs are analyzed together by assuming a weighted mean beam polarization of  $(79.3 \pm 2.0)\%$ . For the data taking the direction of the beam polarization was changed by switching the polarization in the  $H^-$  ion source [15] with every spill, which has a typical length of 100 s.

The systematic errors due to instrumental asymmetries are studied by comparing the results of the observables, obtained by different methods: in case of the  $\Lambda$  polarization these are the integral method, which is applied in this analysis (see eq. 2), and the weighted sum method,

which is described in [16]. In case of the analyzing power these are the double difference method (eq. 9 of reference [17]), and the method described in eq. 4. The comparison of both methods indicates that the deviations are within the range of their statistical error. Therefore, we assume that the systematic errors are less than or equal to the statistical errors. For the spin transfer measurement, we assume the same systematic error due to instrumental asymmetries as in the former observables. The effect of admixtures of  $pK(\Sigma^0 \rightarrow \gamma\Lambda)$  events is expected to introduce the same amount of systematic errors. With these assumptions the mean absolute systematic error for the  $\Lambda$  polarization is 0.04. For the measurement of the analyzing power and the spin transfer coefficient the uncertainty of the beam polarization has to be added to the systematic errors, the mean value of these systematic errors is 0.05 (absolute value).

### 3 $\Lambda$ polarization $P_N$

#### 3.1 Results

The  $\Lambda$  polarization is given by the following equation:

$$I(\theta^*) = I_0 \cdot (1 + P_N \alpha \cos(\theta^*)) \quad (1)$$

$\theta^*$  is the angle between the direction of the decay proton (in the  $\Lambda$  rest frame) and the normal vector to the plane, which is spanned by the beam proton and the  $\Lambda$  direction.  $\alpha$  is the hyperon decay asymmetry parameter:  
 $\alpha(\Lambda \rightarrow p\pi^-) = 0.642 \pm 0.013$  [18]

From eq. 1 the  $\Lambda$  polarization is calculated by applying the difference of the count rates with  $N_A: \cos(\theta^*) > 0$  and  $N_B: \cos(\theta^*) < 0$ :

$$P_N = \frac{2}{\alpha} \frac{N_A - N_B}{N_A + N_B} \quad (2)$$

For the beam momentum of 2.70 GeV/c 227,000 events and for the beam momentum of 2.95 GeV/c 206,000 events are analyzed, here runs without beam polarization are included. The  $\Lambda$  polarization is shown in fig. 2 as a function of the scattering angle, on Feynman  $x_F^1$ , and on the transverse momentum. The initial system consists of two identical particles<sup>2</sup>, therefore, the  $\Lambda$  polarization has to change its sign between the backward  $\Lambda$  region and the forward  $\Lambda$  region :

$$\begin{aligned} P_\Lambda(\cos(\vartheta_\Lambda^{\text{cm}})) &= -P_\Lambda(-\cos(\vartheta_\Lambda^{\text{cm}})) \\ P_\Lambda(x_F) &= -P_\Lambda(-x_F) \end{aligned}$$

<sup>1</sup> Feynman  $x_F$  is defined as the ratio of the longitudinal cm momentum to its maximum possible value

<sup>2</sup> this is exactly true only for an unpolarized beam, the polarization of the beam proton violates this symmetry. But the  $\Lambda$  polarization is evaluated by taking the average of the up and down polarization runs. The integrated luminosities with up and down polarization are almost the same.

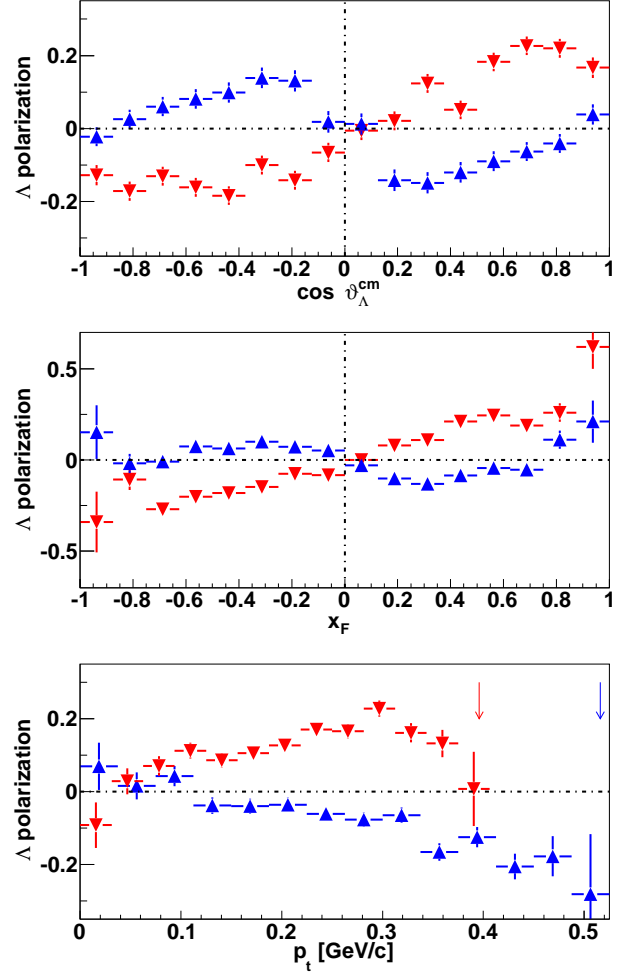


**Fig. 2.** The  $\Lambda$  polarization is shown for two beam momenta: 2.70 GeV/c (red triangles down) and 2.95 GeV/c (blue triangles up). Top: dependence on the  $\Lambda$  cm scattering angle. Middle: dependence on Feynman  $x_F$ . Bottom: dependence on the  $\Lambda$  transverse momentum. For each beam momentum the maximum of the transverse momentum is indicated with arrows in the upper part of the bottom figure.

As the evaluation of the dependence on the transverse momentum averages the  $\Lambda$  polarization of the forward and backward region of the  $\Lambda$ , the resulting polarization would be zero. Therefore, by evaluating the dependence on the transverse momenta, the sign of the polarization for events in the backward region is reversed. The same holds for the dependence on the invariant masses.

The measured  $\Lambda$  polarization is shown in fig. 2 as function of the three kinematic variables. In this and all following figures the error bars indicate the statistical errors. The striking feature of the data is the change of the sign of the polarization between the two beam momentum settings, which is seen in all figures. In the  $\Lambda$  backward region the  $\Lambda$  polarization is negative for the beam momentum of 2.70 GeV/c and positive for the beam momentum of 2.95 GeV/c, for the forward range the signs are

exchanged. This phenomenon has not been observed before. Both curves exhibit within their errors the expected point symmetry for  $\cos\theta^{\text{cm}} = 0$  and  $x_F = 0$ . In addition to the difference in sign, both curves show deviations in the magnitude of the  $\Lambda$  polarization, mainly in the angle region  $0.3 < |\cos\theta^{\text{cm}}| < 1.0$ . In this region the magnitude of the polarization differs up to 80%.

As the variables Feynman  $x_F$  and transverse momentum are not orthogonal, restricted efficiency in one of these variables will effect the value of the  $\Lambda$  polarization in the other variable. For the transverse  $\Lambda$  momentum the COSY-TOF efficiency (acceptance  $\cdot$  reconstruction efficiency) is nearly constant, the variation is less than  $\pm 10\%$ . For the Feynman  $x_F$  variable the acceptance drops in the range of  $|x_F| > 0.8$  from 50% of the maximum acceptance to zero at  $|x_F| = 1$ . However, since the range of  $|x_F| > 0.8$  corresponds to less than 2.8% of the phase space volume, the small fraction of events lying in this range can be neglected for the  $p_t$  distribution.

### 3.2 Comparison with existing data

The full kinematic range of the  $\Lambda$  polarization can only be compared with measurements of DISTO and HADES, which covered a large fraction of the available phase space. The results of these measurements are shown together with the COSY-TOF results in fig. 3. The reaction types and the references are given in table 1. Apart from one data point at  $x_F \sim 0.55$  the DISTO data<sup>3</sup> agree with the COSY-TOF data of 2.95 GeV/c. In dependence on the transverse momentum the HADES data exhibit a negative  $\Lambda$  polarization, similar to the 2.95 GeV/c COSY-TOF results.

As there are conjectures in the literature (see for instance [30]) that the  $\Lambda$  polarization may be independent of the beam momentum and target material, the COSY-TOF results are compared with measurements with beam momenta ranging from near threshold up to 1 TeV/c and with measurements on different target materials. These experiments cover only a small part of the available phase space. The kinematic regions of those measurements, where values of the  $\Lambda$  polarization are accessible for bins in  $x_F$  and  $p_t$ , are summarized in fig. 4. Their range in  $x_F$  and  $p_t$  is indicated by lines. The symbols shown in the legend of fig. 4 are referenced in table 1.

Most of these measurements are inclusive, and thus the separation of directly produced  $\Lambda$  from  $\Sigma^0 \rightarrow \gamma\Lambda$  decay is not possible. The first determination of the  $\Sigma^0$  polarization [31] yields a value of  $\approx 30\%$  and with the opposite sign compared to the  $\Lambda$  polarization. Therefore, the inclusive measurements are expected to reveal a  $\Lambda$  polarization, which is lower than the polarization of the directly produced  $\Lambda$ . The ratio of directly produced  $\Lambda$  to those from the  $\Sigma^0$  decay is dependent on the beam momentum and may be dependent on the kinematical regions of the measurements. The first exclusive measurement of the  $\Lambda$

**Table 1.** Denotation of  $pX \rightarrow \Lambda X$  measurements. The reaction types and the proton beam momenta (for collider experiments the invariant masses) are given.

	reference	reaction and beam momentum
FNAL 1978	[19]	p+Be $\rightarrow \Lambda+X$ 400.9 GeV/c
KEK 1986	[20]	p+Be (Cu,W) $\rightarrow \Lambda+X$ 12.9 GeV/c
CERN ISR 1987	[21]	p+p $\rightarrow \Lambda+X$ $\sqrt{s} = 3\text{--}61$ GeV
AGS 1988 13.5 GeV/c	[8]	p+Be $\rightarrow \Lambda+X$ 13.5 GeV/c
AGS 1988 18.5 GeV/c	[8]	p+Be $\rightarrow \Lambda+X$ 18.5 GeV/c
AGS 1996	[22, 23]	p+p $\rightarrow pK^+\Lambda$ N( $\pi^+\pi^-$ ) 27.5 GeV/c
FNAL 1989	[24]	p+Be (Cu,Pb) $\rightarrow \Lambda+X$ 400.9 GeV/c
FNAL 1991	[25]	p+p $\rightarrow pK^+\Lambda$ 800.9 GeV/c
FNAL 1994	[26]	p+Be $\rightarrow \Lambda+X$ 800.9 GeV/c
DISTO 1998	[5]	p+p $\rightarrow pK^+\Lambda$ 3.67 GeV/c
CERN NA48 1999	[27]	p+Be $\rightarrow \Lambda+X$ $\sqrt{s} = 61$ GeV
HERA-B 2006	[28]	p+C(W) $\rightarrow \Lambda+X$ 920.9 GeV/c
HADES 2014	[4]	p+Nb $\rightarrow \Lambda+X$ 4.34 GeV/c
ATLAS 2015	[29]	p+p $\rightarrow \Lambda+X$ $\sqrt{s} = 7$ TeV

polarization of the reaction  $pp \rightarrow pK^+\Lambda$  at CERN [32] yielded values up to 60%, which are significantly larger than the results obtained by the inclusive measurements. The high polarization values were confirmed by an exclusive measurement at FNAL [25].

In order to incorporate the restricted ranges of the measurements given in fig. 4, the results of COSY-TOF are recalculated for 4 ranges in  $x_F$  and compared with values of the literature, which are inside these ranges (see fig. 5).

For each interval in  $x_F$  a line fit is applied to the COSY-TOF data. The results are given in table 2. The inclination of the 2.70 GeV/c data fit is positive for all  $x_F$  intervals and rises with  $x_F$ . The inclination of the 2.95 GeV/c data fit is negative and within the errors the same in the first three  $x_F$  intervals. For the extreme  $\Lambda$  forward and backward range ( $|x_F| > 0.7$ ) it is compatible with zero. No systematic agreement with the data from literature can be detected. Nearly all measurements of the literature show a negative  $\Lambda$  polarization. Apart from data below  $p_t = 0.6$  GeV/c of one experiment [25] the COSY-TOF 2.70 GeV/c data are the only ones with a positive polarization for all intervals.

The dependence of the  $\Lambda$  polarization on the kaon- $\Lambda$  invariant mass is given by the experiments BNL E766 and

<sup>3</sup> These data are quoted to be preliminary, they are scanned from fig. 8 of reference [5].



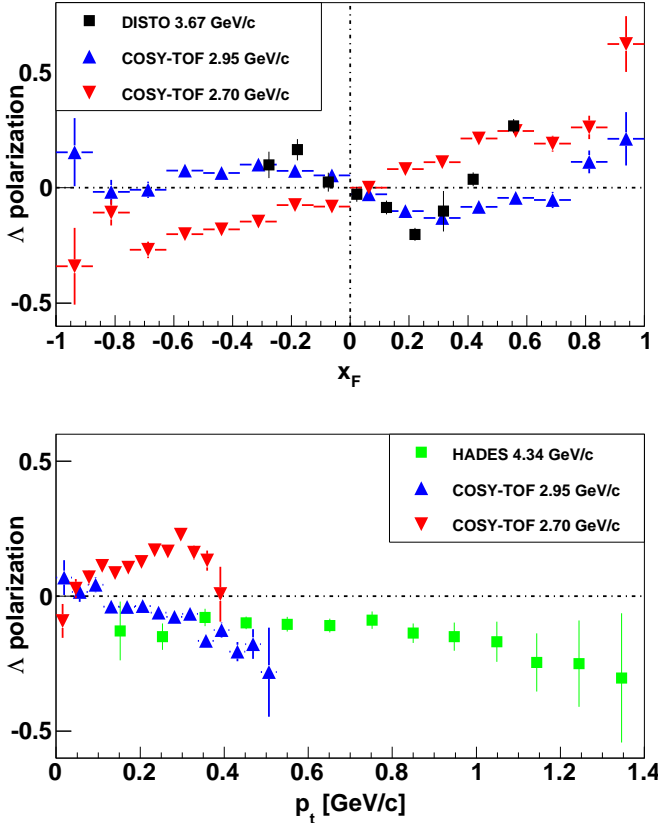


**Fig. 3.** Upper figure: the  $\Lambda$  polarization as a function of Feynman  $x_F$  in comparison to the results of the DISTO experiment. Bottom frame: the  $\Lambda$  polarization as a function of the transverse momentum in comparison to the results of the HADES experiment. The error bars of the HADES data include statistical plus systematic errors. The references for the DISTO and HADES data are given in table 1.

**Table 2.** The results from the line fit in fig. 5 ( $P_N = a_1 \cdot p_t [\text{GeV}/c]$ )

data range $ x_F $	$a_1 [(\text{GeV}/c)^{-1}]$	
	$p_b = 2.70 \text{ GeV}/c$	$p_b = 2.95 \text{ GeV}/c$
0.0–0.3	$0.33 \pm 0.04$	$-0.33 \pm 0.04$
0.3–0.5	$0.87 \pm 0.06$	$-0.43 \pm 0.05$
0.5–0.7	$1.23 \pm 0.08$	$-0.34 \pm 0.07$
0.7–1.0	$1.59 \pm 0.18$	$0.20 \pm 0.15$

FNAL E690 [25, 33, 34]. These data are compared with the data of COSY-TOF in fig. 6. Since the data of BNL and FNAL are restricted to Feynman  $x_F$  region of  $|x_F| > 0.4$  we apply the same restriction to the COSY-TOF data. The BNL set of data varies by including  $\pi^+\pi^-$  pairs to the  $pK\Lambda$  final state. Only the data with 2 and 4 pions are shown in fig. 6. No obvious similarities between these data sets and the COSY-TOF data can be found. For the sake of completeness the  $\Lambda$  polarization is plotted as a function of the  $p\Lambda$  invariant mass in the lower part of fig. 6. No data in the literature are existing for comparison.

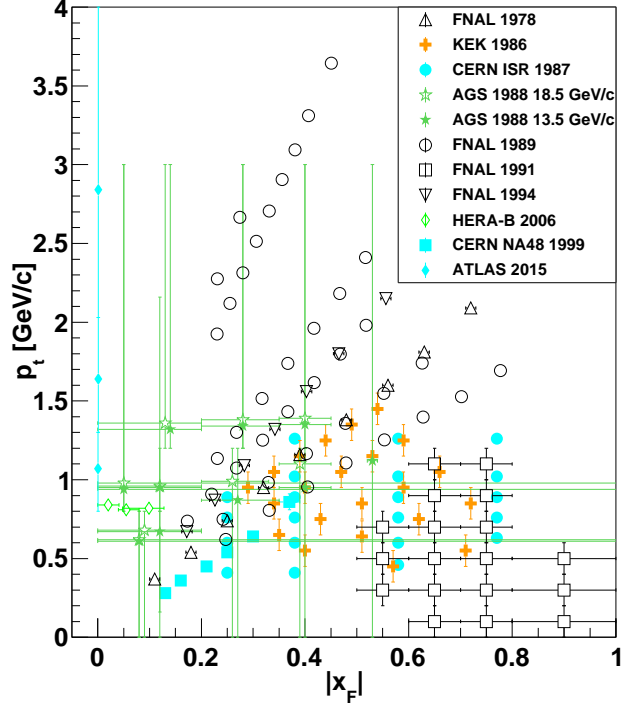


**Fig. 4.** Kinematic regions of  $\Lambda$  polarization measurements, for which the dependence of the  $\Lambda$  polarization on the transverse momentum and on Feynman  $x_F$  are explicitly given. The bin width of the measurements are indicated by error bars. The references for the measurements are given in table 1.

### 3.3 Dependence of the $\Lambda$ polarization on the cm momentum

In order to describe the variation of the  $\Lambda$  polarization with  $\cos\vartheta_\Lambda^{\text{cm}}$  by only two parameters, the  $\Lambda$  polarization is multiplied with the differential cross section and fitted with the sum of the associated Legendre polynomials  $L_2^1$  and  $L_4^1$ :

$$P_N(\cos\vartheta_\Lambda^{\text{cm}}) \cdot \frac{d\sigma_0}{d\Omega} = b_2 L_2^1(\cos\vartheta_\Lambda^{\text{cm}}) + b_4 L_4^1(\cos\vartheta_\Lambda^{\text{cm}}) \quad (3)$$

$d\sigma_0/d\Omega$  is the spin averaged differential cross section, it is determined as described in sec. 4.3. These polynomials are chosen as they have the required roots and point symmetry.  $L_2^1$  describes the data with a structure of one maximum/minimum each in the forward and backward region, while the polynomial  $L_4^1$  has two maxima/minima in each region. The data are divided into six bins of the  $\Lambda$  cm momentum, as shown by the error bars at the abscissa in fig. 7 and fit according to eq. 3. The fit results do not improve by adding the  $l = 6$  Legendre polynomial, which would add structures with three maxima/minima in each region. The variation of the coefficients  $b_2$  and  $b_4$  with the cm momentum are shown in fig. 7 for both beam momenta.

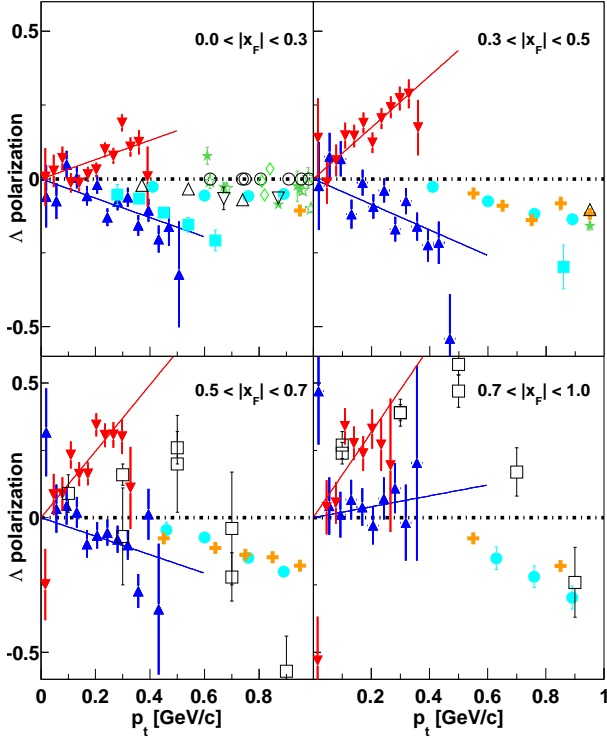


**Fig. 5.** Comparison of the COSY-TOF data (blue, filled triangles up for 2.95 GeV/c and red, filled triangles down for 2.70 GeV/c) with data from literature, the symbols are the same as in fig. 4. For better visibility error bars of the abscissa are not plotted. The range of Feynman  $x_F$  is indicated in the figures. The COSY-TOF data have been fit with a straight line, the fit parameters are given in table 2.

For the 2.70 GeV/c data the coefficient  $b_4$  is constant and close to zero within the error bars, while the magnitude of the coefficient  $b_2$  increases nearly linearly with the  $\Lambda$  cm momentum. For the 2.95 GeV/c data the magnitudes of both coefficients rise with the momentum. The distribution and fit for each momentum bin is shown in the appendix A in figs. 15, 16.

## 4 Analyzing power $A_N$

### 4.1 Results

The analyzing power  $A_N$  describes the left-right asymmetry of the final state particles originated by the vertical beam polarization. The analyzing power is determined by applying the following equation:

$$A_N = \frac{1}{P_B \cdot \cos(\varphi)} \cdot \frac{N^\uparrow(\varphi) - N^\downarrow(\varphi)}{N^\uparrow(\varphi) + N^\downarrow(\varphi)} \quad (4)$$

$\varphi$  is the azimuth angle.  $N$  denotes the count rates and  $\uparrow, \downarrow$  indicate the direction of the beam polarization.  $P_B$  is the

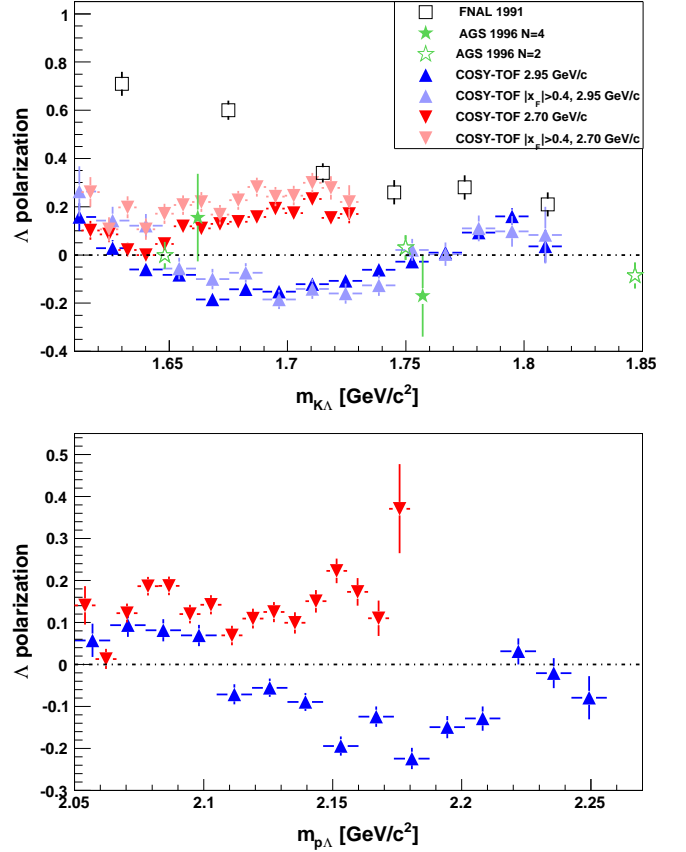


**Fig. 6.** Top: comparison of the  $\Lambda$  polarization as a function of the  $K\Lambda$  invariant mass. In order to show the effect of the restriction of the data to the range of Feynman  $x_F$  as in the literature data, the COSY-TOF data are plotted with and without this restriction. In the legend of the AGS data  $N$  gives the number of  $\pi^+\pi^-$  pairs which are evaluated together with  $pK\Lambda$ . Bottom: COSY-TOF data of the  $\Lambda$  polarization as a function of the  $p\Lambda$  invariant mass.

absolute value of the beam polarization. Three beam proton analyzing powers can be determined:  $A_N(\varphi^p)$ ,  $A_N(\varphi^K)$ , and  $A_N(\varphi^\Lambda)$  depending on which final state particle is considered.

In contrast to the  $\Lambda$  polarization, the symmetry of the initial system is broken, since the beam proton is polarized. Therefore, no symmetry in the functional dependence on the scattering angle and on the Feynman  $x_F$  are expected. The following boundary conditions are given:  $A_N(|\cos(\vartheta^{cm})| = 1) = 0$  and  $A_N(|x_F| = 1) = 0$ . As the minimum of the transverse momentum corresponds to  $|\cos(\vartheta^{cm})| = 1$ , the analyzing power at  $p_t = 0$  GeV/c must be zero too.

The results of the analyzing power measured by the proton, kaon and  $\Lambda$  asymmetries are shown in fig. 8. The analyzing powers are given as a function of the cm scattering angle, the Feynman  $x_F$ , and the transverse momentum of the corresponding final state particle.

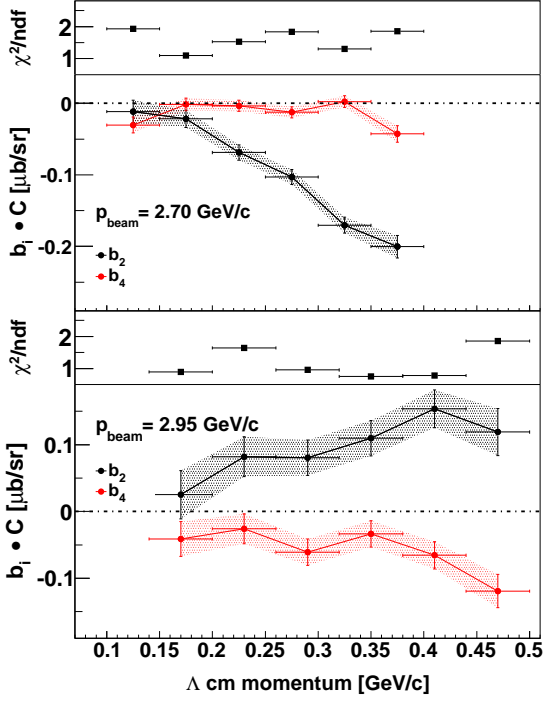


**Fig. 7.** The variation of the Legendre coefficients  $b_2$  (black) and  $b_4$  (red) as defined in eq. 3 with the cm  $\Lambda$  momentum. The upper figure contains the data of 2.70 GeV/c beam momentum, the lower contains the 2.95 GeV/c data. Above each figure is the reduced  $\chi^2$  of the fit.

While the analyzing power generating the p and  $K^+$  asymmetries does not change significantly with the beam momentum, larger differences are found for the analyzing power from the  $\Lambda$  asymmetry. The analyzing power of the proton and of the  $\Lambda$  asymmetry are mainly negative, while the analyzing power of the kaon asymmetry is essentially positive. For transverse momenta below 0.25 GeV/c the analyzing power of the proton asymmetry is nearly zero and decreases linearly to  $-0.2$  above this momentum. The analyzing power of the kaon asymmetry shows an inverse behavior: for momenta below 0.25 GeV/c it increases nearly linearly from 0 to 0.10 and it is constant above this momentum.

#### 4.2 Comparison with existing data

The analyzing power has only been measured exclusively for the associated strangeness production by DISTO and COSY-TOF. The DISTO data were measured at beam momenta of 3.67 GeV/c, 3.31 GeV/c, and 2.94 GeV/c [35, 36]. The analyzing power determined with the  $\Lambda$  asymmetry of the 2.94 GeV/c data<sup>4</sup> are compared in fig. 9 with the COSY-TOF data of 2.95 GeV/c as a function of the

<sup>4</sup> The data are scanned from fig. 4 of reference [35], they are quoted to be preliminary.

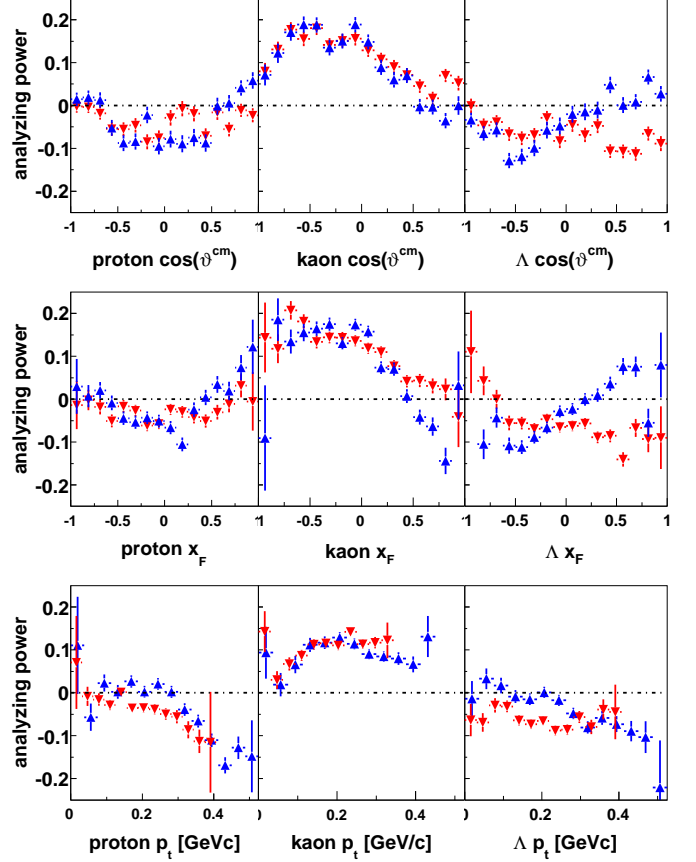


**Fig. 8.** The analyzing power is shown for two beam momenta: 2.70 GeV/c (red triangles down) and 2.95 GeV/c (blue triangles up). Top: dependence on the cm scattering angle. Middle: dependence on the Feynman  $x_F$ . Bottom: dependence on the transverse momentum.

scattering angle, Feynman  $x_F$ , and the transverse momentum. While the dependence on the transverse momentum of both data sets exhibits a similar behavior, discrepancies are seen in  $\cos\theta^{\text{cm}}$  and  $x_F$ : for the forward range the DISTO data yield a negative analyzing power, the COSY-TOF data have positive values.

A subset of the COSY-TOF data, which had been measured in 2010 was evaluated in [14] for the determination of the spin triplet  $p\Lambda$  scattering length. The comparison of the analyzing power of the kaon asymmetry is given in the last plot of fig. 9. Both analyses exhibit consistent characteristics of this analyzing power.

#### 4.3 Description with Legendre polynomials:

The differential cross section of proton-proton interactions with a beam polarization  $P_B$  in the  $\pm y$  direction and an unpolarized target, is given by ([37,38]):

$$\frac{d\sigma(\cos\vartheta^*)}{d\Omega} = \frac{d\sigma_0(\cos\vartheta^*)}{d\Omega} + P_B \frac{d\sigma_y(\cos\vartheta^*)}{d\Omega} \quad (5)$$

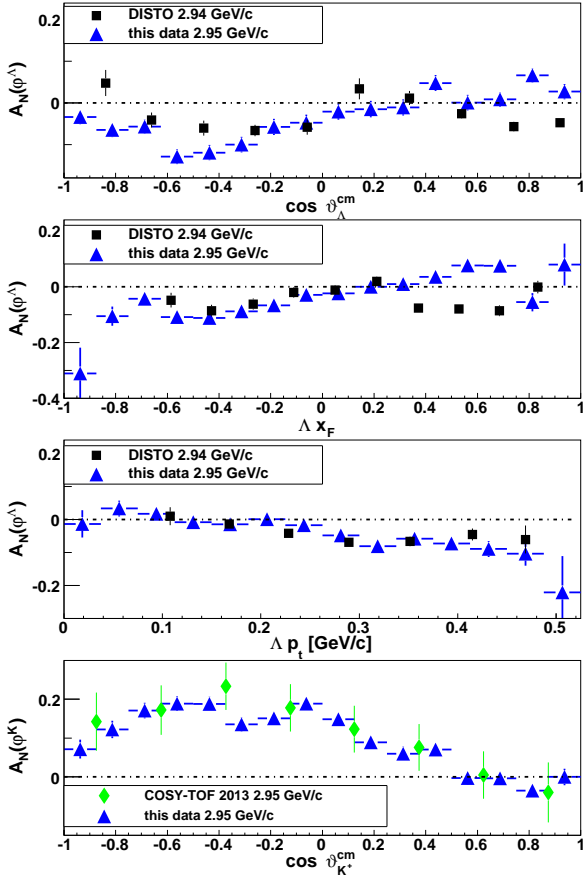


**Fig. 9.** In the top three figures the analyzing power measured at 2.95 GeV/c are compared with data from DISTO, which were measured at 2.94 GeV/c [35]. The bottom figure compares the analyzing power of the kaon asymmetry at 2.95 GeV/c with a previous analysis including only 20% of the COSY-TOF data [14].

$d\sigma_0(\cos\vartheta^*)/d\Omega$  is the spin averaged differential cross section and  $d\sigma_y(\cos\vartheta^*)/d\Omega$  is the spin dependent cross section. The analyzing power  $A_N$  is given by

$$A_N = \frac{d\sigma_y(\cos\vartheta^*)/d\Omega}{d\sigma_0(\cos\vartheta^*)/d\Omega} \quad (6)$$

The differential cross sections can be expressed by a sum of Legendre polynomials:

$$\begin{aligned} d\sigma_0(\cos\vartheta^*)/d\Omega &= \frac{1}{4\pi} \sum_n a_n L_n^0 \\ d\sigma_y(\cos\vartheta^*)/d\Omega &= \frac{1}{4\pi} \sum_n b_n L_n^1 \end{aligned} \quad (7)$$

$L_n^0$  ( $L_n^1$ ) are the associated Legendre functions of order 0 (1).  $a_n$  are the related coefficients of order 0,  $n = 0, 1, 2, \dots$  and  $b_n$ ,  $n = 1, 2, 3, \dots$  are the related coefficients of order 1. In order to determine the coefficients  $b_n$ , the product of the analyzing power and the unpolarized cross section  $A_N \cdot d\sigma_0/d\Omega$  is fit with the  $n = 1, 2, 3$  associated Legendre functions. The unpolarized cross section  $d\sigma_0/d\Omega$  is

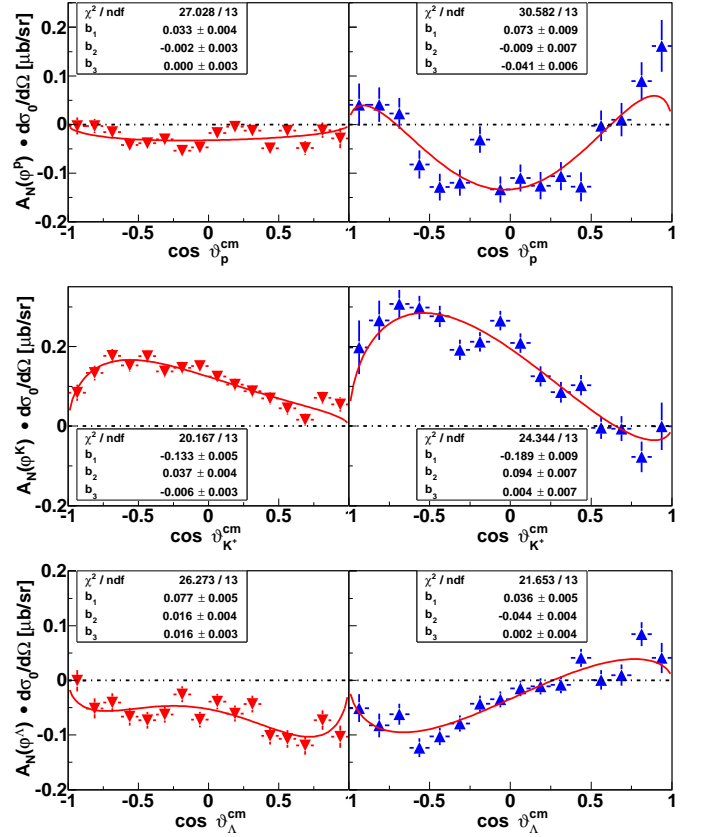


**Fig. 10.** The product of the analyzing power and the unpolarized cross section  $A_N \cdot d\sigma_0/d\Omega$  for the three final state particles is shown by the triangles, left column for 2.70 GeV/c beam momentum, right column for 2.95 GeV/c beam momentum. The fit results for the sum of the Legendre polynomials are shown by the red lines. The values of the coefficients  $b_i$  are given in the figures.

determined by fitting the angular distribution (see fig. 3 in reference [1]) with associated Legendre functions of order 0 up to the degree of  $n = 2$ . The fit results of  $A_N \cdot d\sigma_0/d\Omega$  are shown in fig. 10.

In contrast to proton-proton reactions with two particles in the final state – e.g.  $pp \rightarrow d\pi^+$  – no direct conclusions on the partial waves can be drawn from the composition of the Legendre coefficients.

#### 4.4 Dependence of the Legendre Coefficients on the particle momenta

In order to determine the dependence of the Legendre coefficients on the particle cm momentum, the data are divided into six bins of the particle momentum. For each bin the analyzing power distribution is calculated and fit with the Legendre polynomials  $L_n^1$  ( $n = 1, 2, 3$ ). The distributions of the analyzing power and the fit in each bin are shown in the appendix A in figs. 17 - 22. The range of the momentum of each bin is indicated in the plots.



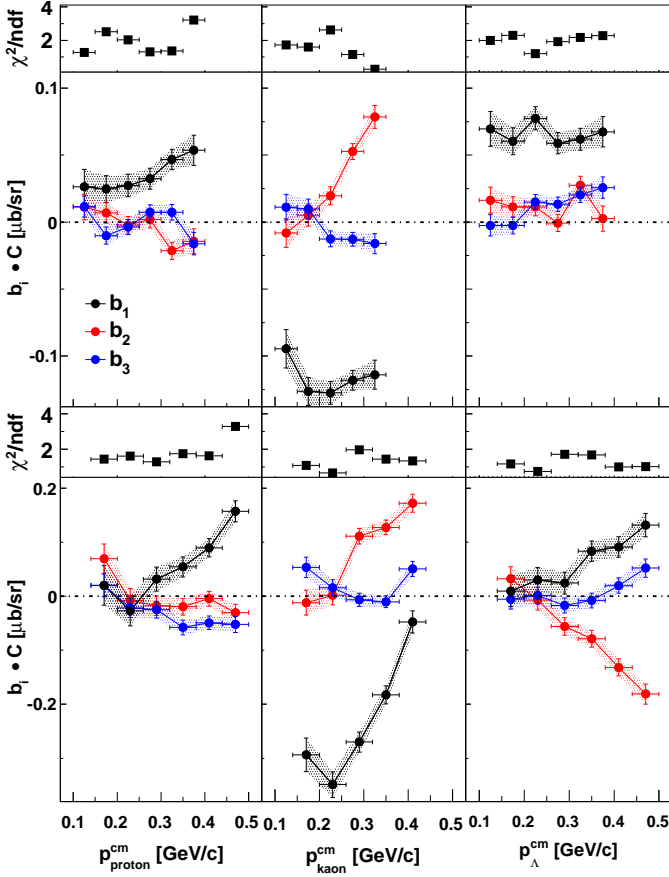


**Fig. 11.** Legendre coefficients obtained by fitting the analyzing power plotted as a function of the cm momenta. The coefficients are distinguished by the color code: black:  $b_1$ , red:  $b_2$ , and blue:  $b_3$ . The values are plotted for 2.70 GeV/c (top row) and 2.95 GeV/c (bottom row). The reduced  $\chi^2$  values of the fits are shown above each figure.

The momentum dependence of the coefficients is shown in fig. 11.

By omitting the coefficients  $b_2$ ,  $b_3$  or both in the fit and by comparing the reduced  $\chi^2$  of these fits it is observed that below cm momenta of 200–300 MeV/c the analyzing power can be described with the first Legendre polynomial alone. Above this momentum the analyzing power of the proton asymmetry needs the third Legendre polynomial and the analyzing power of the  $\Lambda$  and kaon asymmetry need the second Legendre polynomial.

From fig. 11 it can be seen that the determination of the spin triplet  $\Lambda$  proton scattering length from the  $p\Lambda$  invariant mass distribution and the analyzing power from the kaon asymmetry (the method is developed in ref. [39]) is only possible for the data taken at 2.70 GeV/c: the variation of the first Legendre coefficient  $b_1$  with the invariant mass  $p\Lambda$  for low invariant masses is needed. (For details see [14, 40]). This low  $M_{p\Lambda}$  range corresponds to high kaon cm momenta. For the data at 2.95 GeV/c (lower row of fig. 11) the coefficient  $b_1$  is close to zero for the highest kaon cm momenta ( $-0.05 \pm 0.02$ ), thus its dependence on the

low mass part of the invariant mass can not be determined with the required precision. In contrast, for the 2.70 GeV/c data this coefficient is  $-0.14 \pm 0.02$  and nearly constant for the high kaon cm momentum range (upper row of fig. 11), a necessary condition to evaluate the spin triplet  $\Lambda$  proton scattering length.

## 5 Spin transfer coefficient: $D_{NN}$

### 5.1 Results

The transfer of the beam-proton polarization to the hyperon is quantified by the spin transfer coefficient  $D_{NN}$ . The common definition (see for instance [8]) implies that it is positive if the polarization of the hyperon is aligned with the beam polarization, negative if the hyperon polarization is oriented opposite to the beam polarization and zero, if the hyperon polarization is independent of the beam polarization.

The spin transfer coefficient is calculated with the following formula:

$$D_{NN}(\vartheta^*) = \frac{4}{\alpha P_B} \epsilon_D(\vartheta^*) \quad (8)$$

$\alpha$  is the  $\Lambda$  decay asymmetry parameter  $\alpha(\Lambda \rightarrow p\pi^-) = 0.642 \pm 0.013$  [18],  $P_B$  the magnitude of the beam polarization, and  $\epsilon_D(\vartheta^*)$  is calculated from the differences of count rates depending on the orientation of the beam polarization, the  $\Lambda$  polarization, and the hemisphere of the detector. For a detailed discussion see ref. [41].

The spin transfer coefficient  $D_{NN}$  is shown in fig. 12 as a function of the  $\Lambda$  scattering angle, Feynman  $x_F$ , and the transverse momentum of the  $\Lambda$ . The measurements show that the coefficient  $D_{NN}$  is negative for nearly all regions, thus the hyperon polarization is opposite to the beam polarization. It is mainly constant as a function of the scattering angle and of Feynman  $x_F$  within the interval of  $x_F = [-0.4, +1.0]$ . For the 2.70 GeV/c data the dependence of  $D_{NN}$  on the transverse momentum can be described by a linear increase of with slope  $(1.3 \pm 0.2) (\text{GeV}/c)^{-1}$  starting with  $-0.6$  at  $p_t = 0 \text{ GeV}/c$ . This behavior is not repeated for the data of 2.95 GeV/c beam momentum, where the fit gives a gradient consistent with zero.

### 5.2 Comparison with existing data

The first measurement of the spin transfer coefficient of  $pp \rightarrow \Lambda X$  was performed in 1975 at a beam momentum of 6 GeV/c [42].  $D_{NN}$  was measured to be  $\approx 0$  for Feynman  $x_F < 0.6$  and for  $x_F > 0.6$  to be  $\approx -0.5$ . The range of the corresponding transverse momentum is not given in the paper and the contamination with  $\Lambda$ 's of the  $\Sigma^0$  decay is not discussed. In 1988  $D_{NN}$  was measured at beam momenta of 13.3 GeV/c and 18.5 GeV/c with a beryllium target [8]. The range of the transverse momentum was up to 3 GeV/c, with Feynman  $x_F$  mainly in the forward range. The ratio of  $\Lambda$  from the  $\Sigma^0$  decay to direct production was estimated to be 40%. For the whole range of the

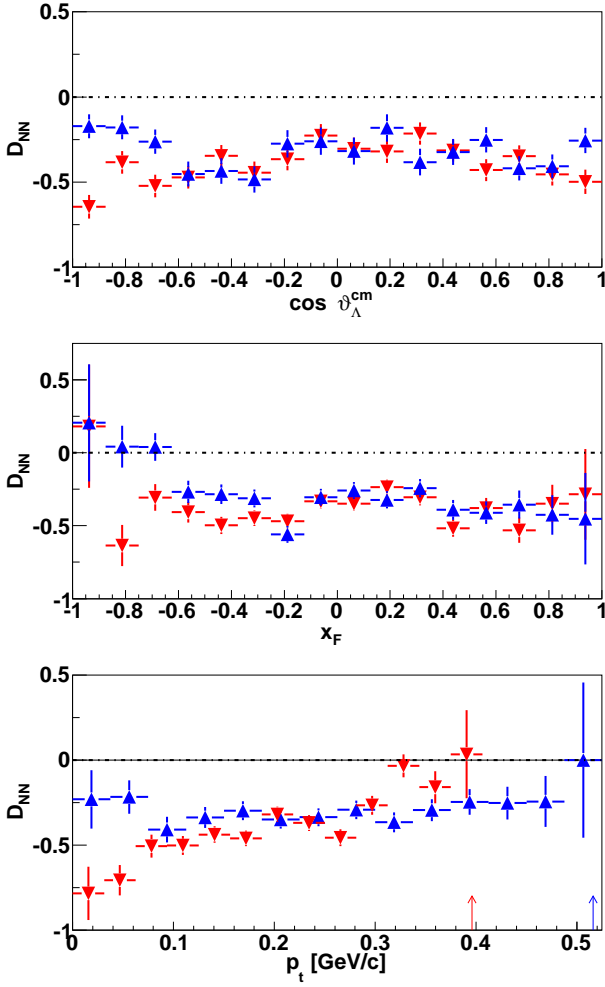


**Fig. 12.** Spin transfer coefficient for 2.70 GeV/c (red triangles down) and 2.95 GeV/c (blue triangles up). Top: dependence on the  $\Lambda$  cm scattering angle. Middle: dependence on the  $\Lambda$  Feynman  $x_F$ . Bottom: dependence on the  $\Lambda$  transverse momentum. For both beam momenta the maxima of the transverse momenta are indicated with arrows in the lower part of the figure.

measurements no significant deviations of  $D_{NN}$  from zero were found. A third measurement with a beam momentum of 200 GeV/c and a liquid hydrogen target covered the forward range of  $x_F$  [9]. The fraction of  $\Lambda$ 's from  $\Sigma^0$  decay is not discussed in the paper.  $D_{NN}$  was measured to be compatible with zero for  $0.1 \text{ GeV/c} < p_t < 0.6 \text{ GeV/c}$ , and for  $0.6 \text{ GeV/c} < p_t < 1.5 \text{ GeV/c}$   $D_{NN}$  is positive and in the range of 0.3–0.4. The results of these measurements are not in agreement with the present data and they exhibit no consistent dependence on Feynman  $x_F$ . Therefore, it cannot be determined, how strongly the polarization transfer depends on the beam momentum. The first exclusive measurements of the polarization transfer were performed by the DISTO experiment [35].  $pK\Lambda$  and  $pK\Sigma^0$  events are identified in the  $pK$  missing mass spectrum, the admixture of  $\Lambda$  from  $\Sigma^0$  decay is lower than 30% [10] for

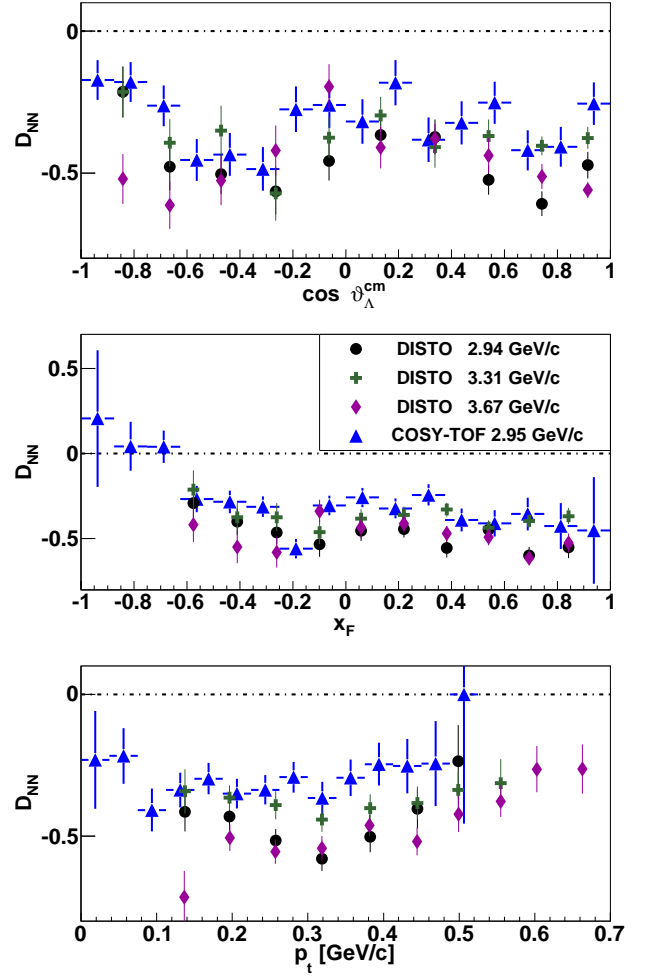


**Fig. 13.** The spin transfer coefficient is shown for the DISTO data [35] and the 2.95 GeV/c COSY-TOF data. For a better clarity of the figure, the 2.70 GeV/c data of COSY-TOF are omitted in this figure. Top: dependence on the  $\Lambda$  cm scattering angle. Middle: dependence on the  $\Lambda$  Feynman  $x_F$ . Bottom: dependence on the  $\Lambda$  transverse momentum.

the beam momentum of 3.67 GeV/c. These data are compared with the COSY-TOF results of  $p_b = 2.95 \text{ GeV/c}$  in fig. 13. Both data sets exhibit a negative  $D_{NN}$ , which is approximately constant. The magnitude of  $D_{NN}$  measured by COSY-TOF is smaller compared with the DISTO data. The mean value of the COSY-TOF data in the  $x_F$  range of  $[-0.5, +1.0]$  is  $-0.37 \pm 0.02$ , the corresponding mean value of the DISTO data is  $-0.46 \pm 0.01$ . The mean values of each measurement are given in table 3.

The indication of the COSY-TOF data that  $D_{NN}$  changes to positive values for  $x_F < -0.6$  cannot be confirmed by the DISTO data, as the acceptance of this detector for that range is too small [43].

**Table 3.** Mean values of  $D_{NN}$  for  $x_F = [-0.5, +1.0]$ 

data set	$\overline{D_{NN}}$
DISTO 2.94 GeV/c	$-0.50 \pm 0.02$
DISTO 3.31 GeV/c	$-0.38 \pm 0.02$
DISTO 3.67 GeV/c	$-0.50 \pm 0.02$
COSY-TOF 2.70 GeV/c	$-0.39 \pm 0.02$
COSY-TOF 2.95 GeV/c	$-0.34 \pm 0.02$

### 5.3 Comparison with model calculations

As developed by Laget [44] the dependence of the spin transfer coefficient on the Feynman  $x_F$  can be characterized by assuming pion or kaon exchange mechanism for the associated strangeness production. For pion exchange the upper vertex in the Feynman diagram of fig. 14 is  $p + \pi \rightarrow K^+ + \Lambda$ . Both sides of this vertex have negative parity, if internal angular momenta are 0. For a polarized beam proton, the  $\Lambda$  spin will have the same direction as the proton spin ( $D_{NN} = +1$ ). In case of a kaon exchange

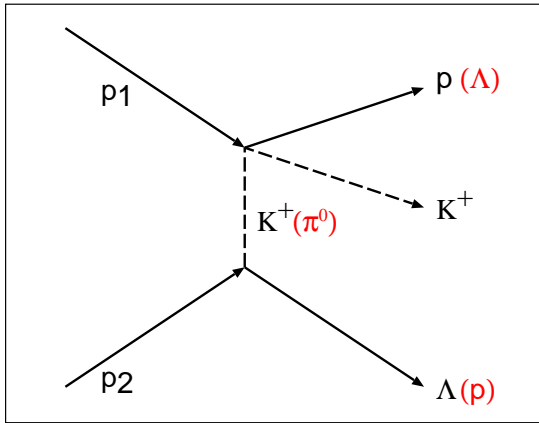


**Fig. 14.** Feynman graph of the associated strangeness production, with either kaon exchange or pion exchange (red symbols in brackets).  $p_{1,2}$  are the beam and target proton, their order can be exchanged.

the lower vertex in the Feynman diagram is given by  $p \rightarrow K^+ + \Lambda$ . Here the parity changes, therefore, the  $\Lambda$  spin has to be opposite compared to the beam proton polarization direction ( $D_{NN} = -1$ ). For backward  $\Lambda$  regions the  $\Lambda$  is essentially produced on the unpolarized target proton. Thus, in this region  $D_{NN}$  is expected to be zero.

As the data exhibit for  $x_F > 0$   $D_{NN} \approx -0.3$ , the conclusion from the Laget model indicates the existence of a mixture of kaon and pion exchange mechanism. The backward region exhibits the same value for  $D_{NN}$ , only for  $x_F < -0.6$  the 2.95 GeV/c data give values of  $D_{NN}$ , which are compatible with zero. A newer calculation [45] considers in addition the exchange of a  $\rho$  meson. It is shown that  $D_{NN}$  can have negative values without assuming a kaon exchange.  $D_{NN}$  is given as a function of the ratio of the  $\pi$  exchange amplitude ( $D_\pi$ ) to the  $\rho$  exchange amplitude ( $B_\rho$ ). For  $D_{NN} = -0.3$  there are two solutions for this ratio:

$D_\pi/B_\rho = 0.3$  and  $D_\pi/B_\rho = 1.5$  (fig. 3 of ref. [45]). From the same calculation the ratio of the total cross sections  $R = (\text{pn} \rightarrow \text{nK}^+\Lambda) / (\text{pp} \rightarrow \text{pK}^+\Lambda)$  is given in dependence on  $D_\pi/B_\rho$ . With this function the value of  $D_{NN} = -0.3$  is connected to the ratio  $R = 4$  and  $R = 6$ . This ratio will be examined by a future publication, where results from a recently completed measurement with COSY-TOF of  $\text{pn} \rightarrow \text{pK}^0\Lambda$  at a beam momentum of 2.95 GeV/c will be presented.

## 6 Summary

The  $\Lambda$  polarization, the analyzing power determined by the asymmetry of the final state particles, and the  $\Lambda$  spin transfer coefficient are measured exclusively in the reaction  $pp \rightarrow pK^+\Lambda$  at beam momenta of 2.70 GeV/c and 2.95 GeV/c.

It is shown that the  $\Lambda$  polarization changes significantly in its magnitude and sign with the beam momentum. This is the first time that this effect is observed. In contrast to all existing data the 2.70 GeV/c COSY-TOF data exhibit a positive  $\Lambda$  polarization in forward direction. The 2.95 GeV/c data are in agreement with the measurements of DISTO and HADES, but comparisons of the  $\Lambda$  polarization of both beam momenta with data from high beam momentum experiments do not indicate agreement.

In contrast to the  $\Lambda$  polarization the analyzing power does not change significantly with the beam momentum, only the analyzing power measured with the  $\Lambda$  asymmetry differs for these beam momenta. The results at 2.95 GeV/c beam momentum are in agreement with a measurement of DISTO at a beam momentum of 2.94 GeV/c. Apart from the DISTO data no other data exist for comparison. The dependence of the Legendre coefficients on the particle cm momenta yield different behavior between the two beam momenta, especially for the analyzing power measured with the kaon asymmetry.

The measurement of the spin transfer coefficient  $D_{NN}$  yields a negative value of about  $-0.3$ . Apart from the backward region ( $x_F < -0.6$ ) this value does not significantly vary with the beam momentum. The comparison with data from the DISTO experiment yields an agreement of the sign, but the magnitude of  $D_{NN}$  measured with DISTO is about 25% larger compared with the COSY-TOF data. A model calculation, which compares  $\rho$  and  $\pi$  exchange, connects the value of  $D_{NN}$  with the ratio of the cross sections associated strangeness production in pp and pn reactions. The measured value of  $D_{NN}$  implies that this ratio is 4 or 6. This ratio will be determined with existing COSY-TOF data.

The authors want to thank the COSY crew for the excellent beam preparation, J. Uehlemann and N. Paul for the operation of the demanding LH<sub>2</sub> target. This work was supported by grants from Forschungszentrum Jülich (COSY-FFE), by the European Union Seventh Framework program (FP7/2007-2013) under grant agreement 283286, and by the Foundation for Polish Science through the MPD programme. Helpful comments of C. Wilkin are gratefully acknowledged.

## 7 Appendix A

This appendix contains the individual fits of the observables, which are separated into bins of a second observable. Inside each figure the fit results and the range of the second observable are given.

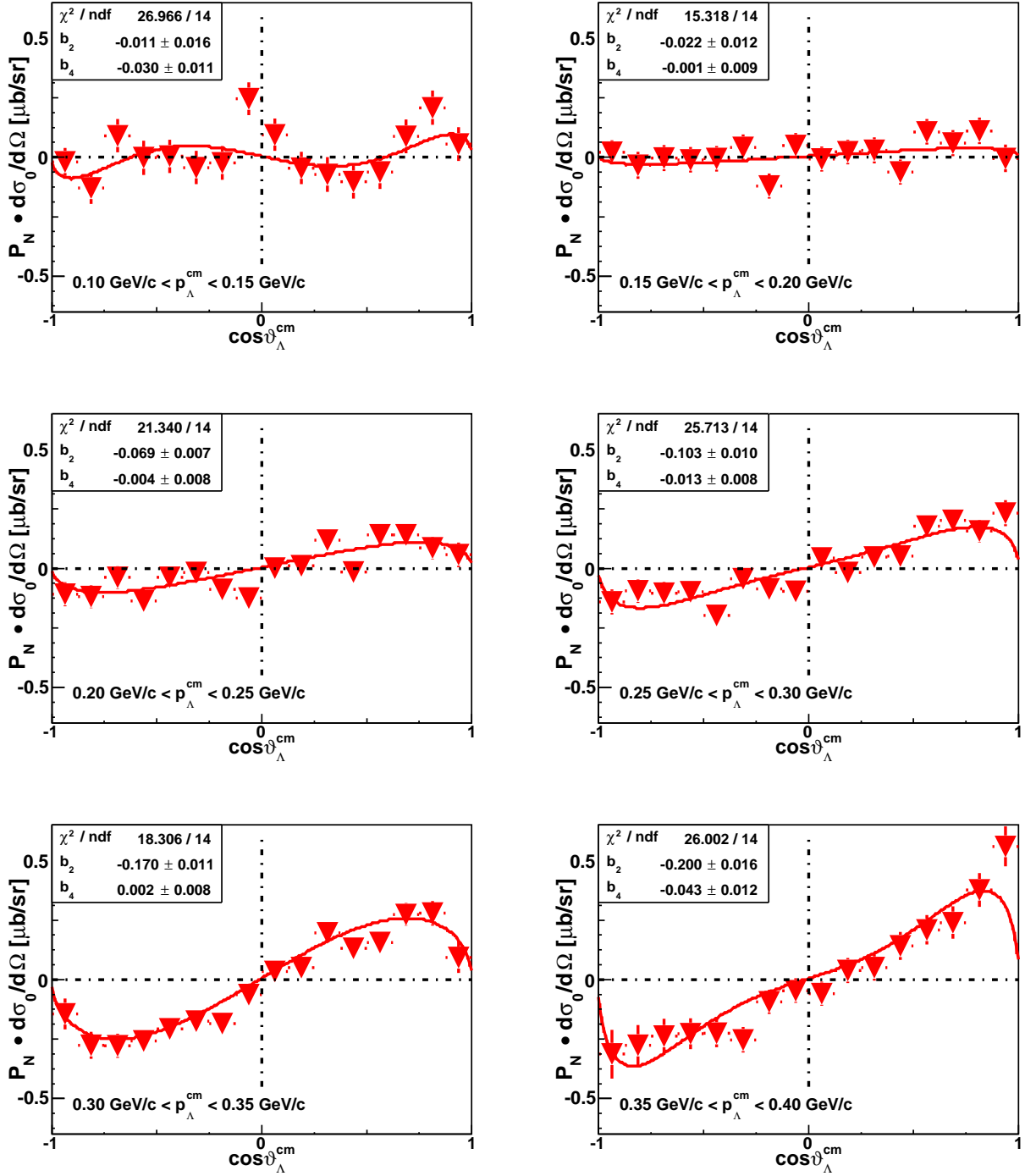


Fig. 15. The  $\Lambda$  polarization multiplied with the differential cross section of the 2.70 GeV/c data is shown for different ranges of the  $\Lambda$  cm momentum. The distributions have been fit with Legendre polynomials according to eq. 3. The fit results and the limits of the  $\Lambda$  cm momenta are given in each figure.



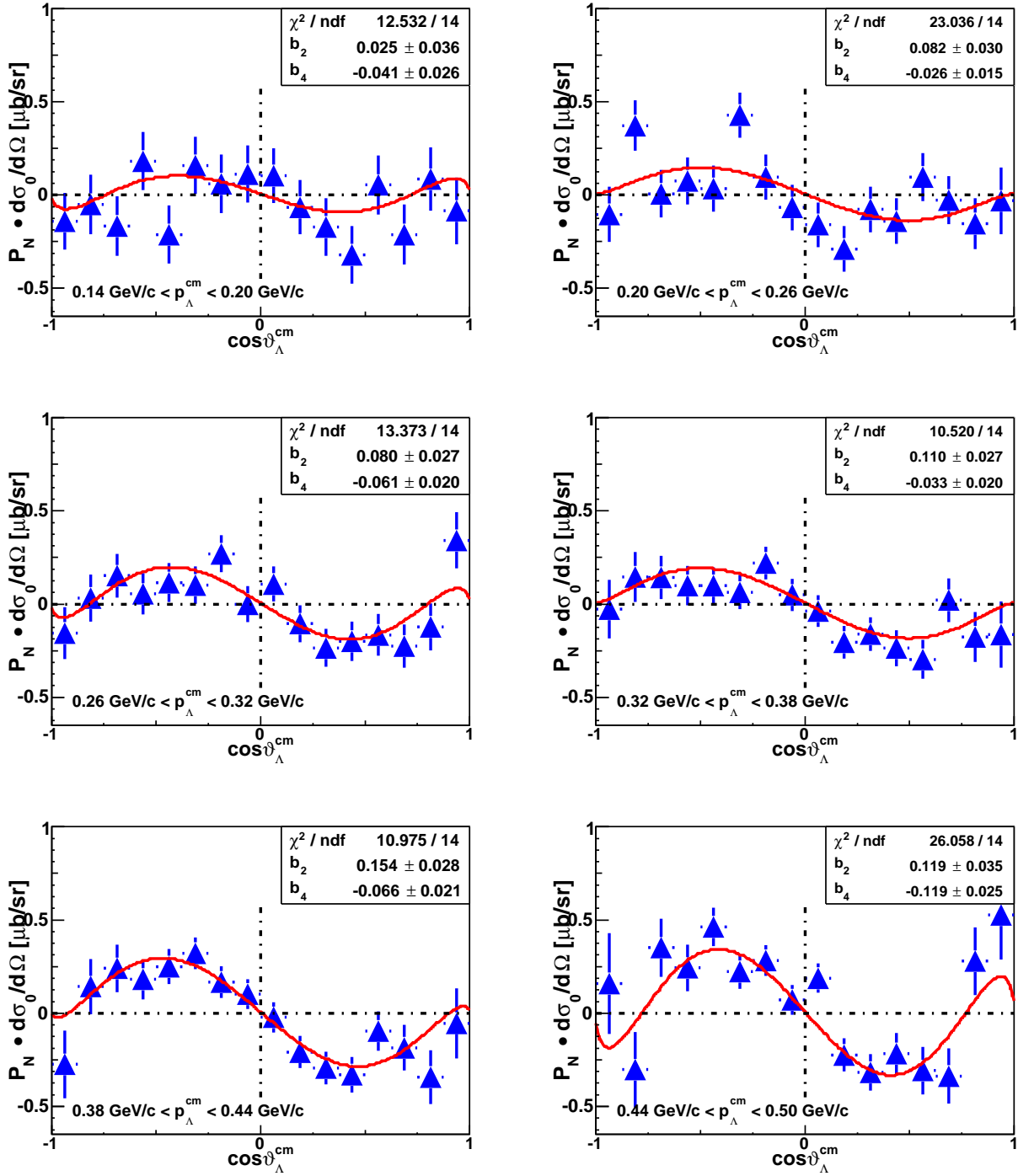
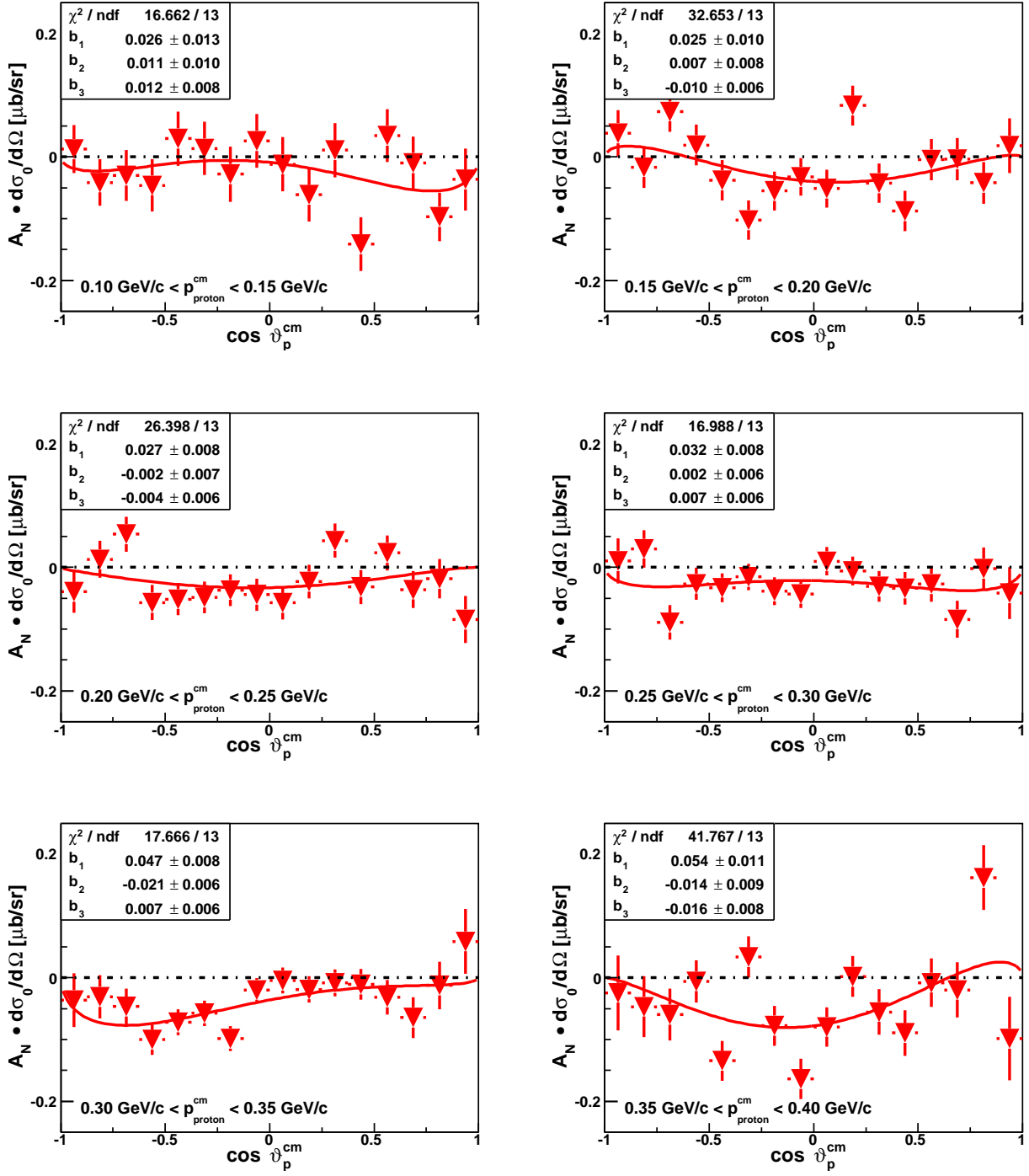
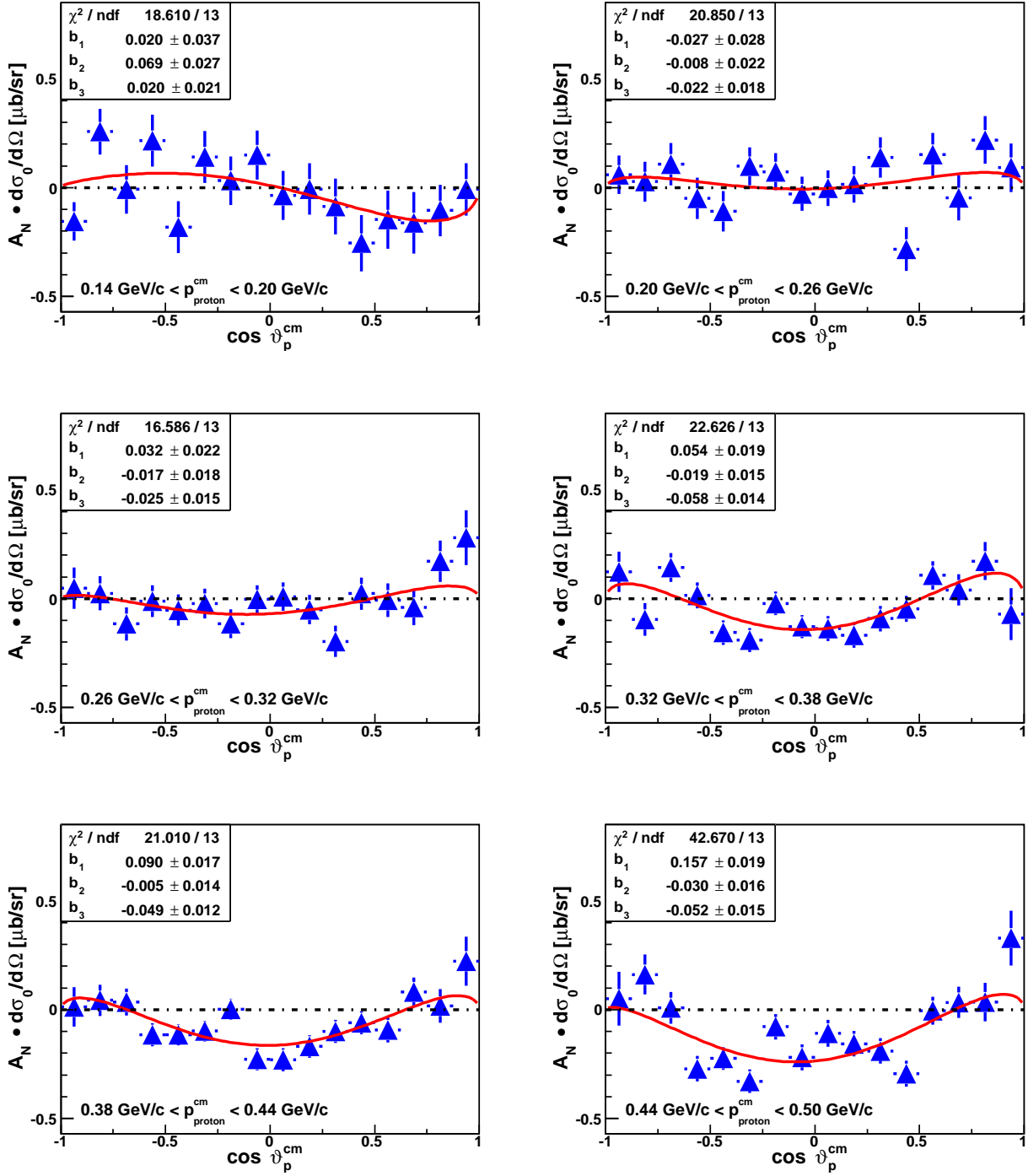


Fig. 16. The  $\Lambda$  polarization multiplied with the differential cross section of the 2.95 GeV/c data is shown for different ranges of the  $\Lambda$  cm momentum. The distributions have been fit with Legendre polynomials according to eq. 3. The fit results and the limits of the  $\Lambda$  cm momenta are given in each figure.



**Fig. 17.** The proton analyzing power multiplied with the differential cross section is shown for different ranges of the proton cm momentum for the 2.70 GeV/c data. The distributions have been fit with Legendre polynomials according to eq. 7. The fit results and the limits of the proton cm momenta are given in each figure.



**Fig. 18.** The proton analyzing power multiplied with the differential cross section is shown for different ranges of the proton cm momentum for the 2.95 GeV/c data. The distributions have been fit with Legendre polynomials according to eq. 7. The fit results and the limits of the proton cm momenta are given in each figure.

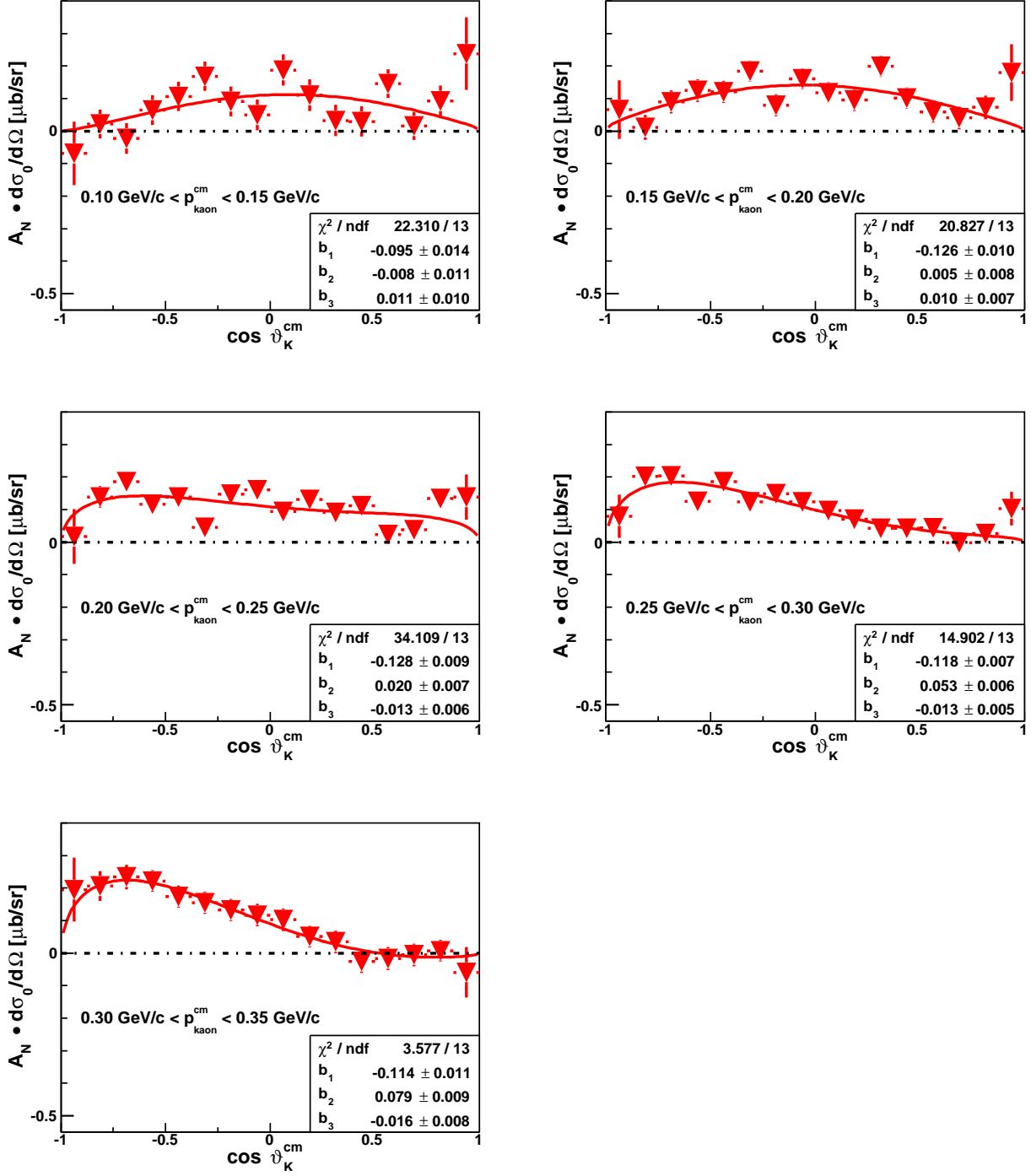


**Fig. 19.** The kaon analyzing power multiplied by the differential cross section is shown for different ranges of the kaon cm momentum for the 2.70 GeV/c data. The distributions have been fit with Legendre polynomials according to eq. 7. The fit results and the limits of the kaon cm momenta are given in each figure.

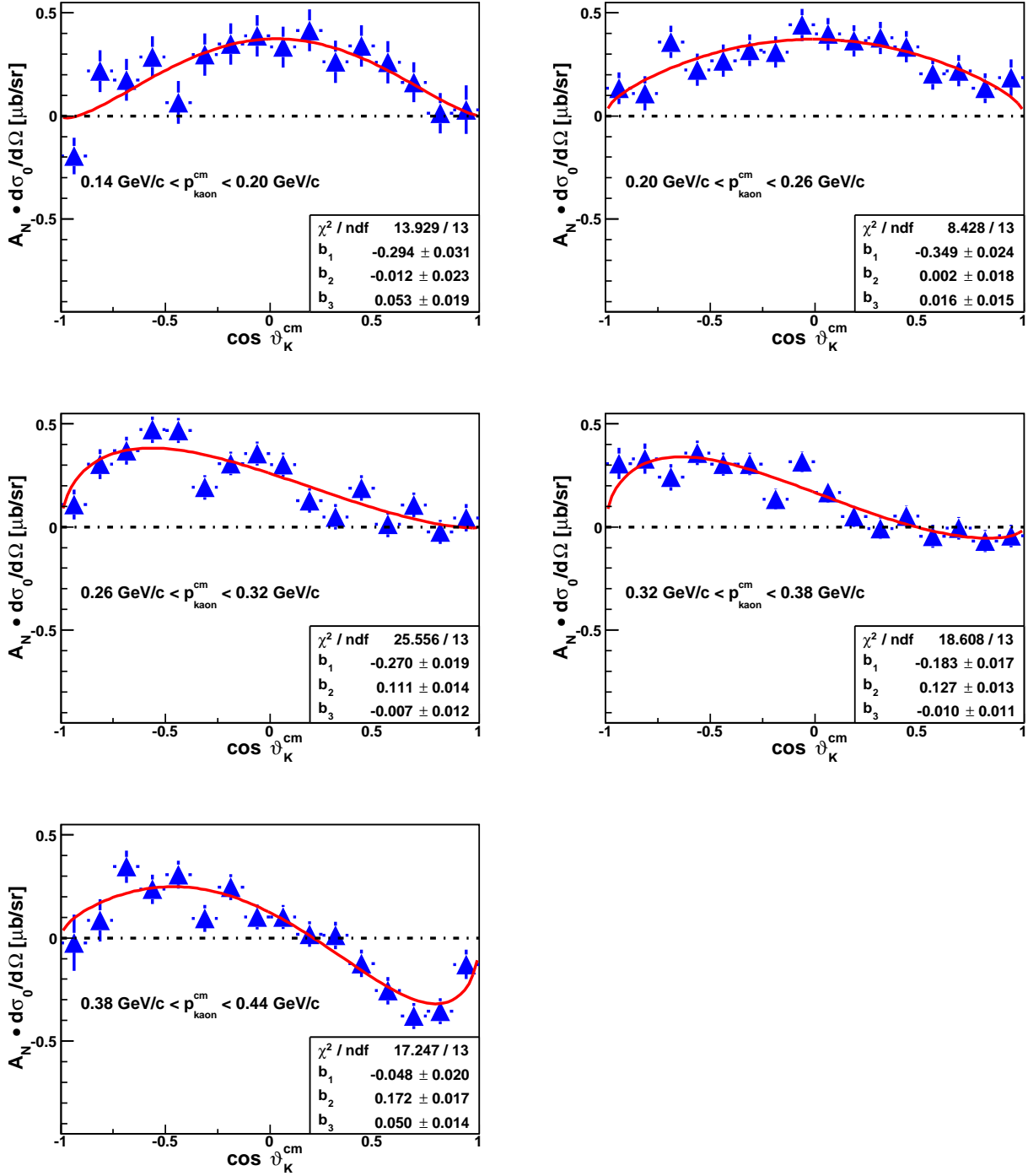


**Fig. 20.** The kaon analyzing power multiplied by the differential cross section is shown for different ranges of the kaon cm momentum for the 2.95 GeV/c data. The distributions have been fit with Legendre polynomials according to eq. 7. The fit results and the limits of the kaon cm momenta are given in each figure.



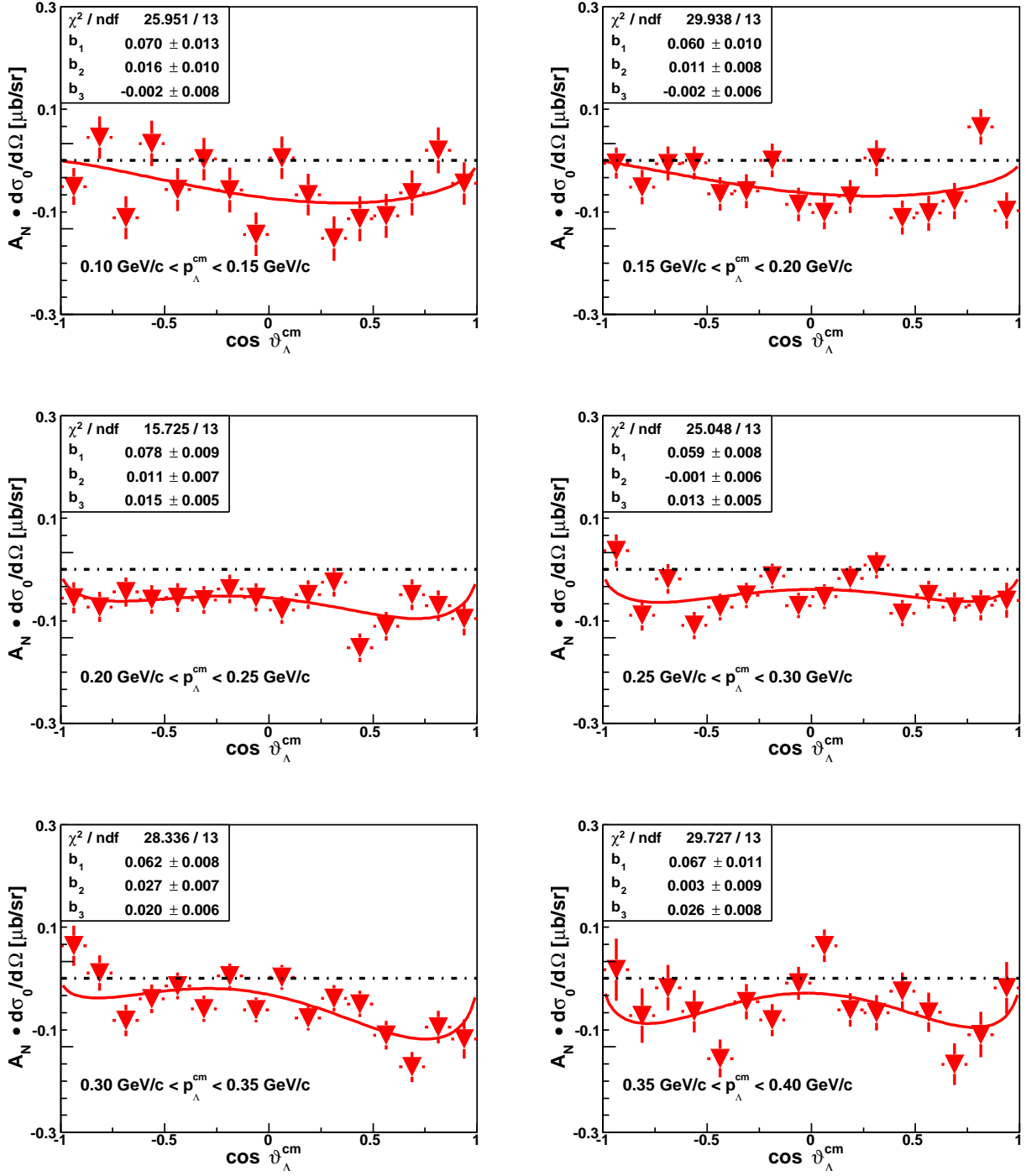


**Fig. 21.** The  $\Lambda$  analyzing power multiplied with the differential cross section is shown for different ranges of the  $\Lambda$  cm momentum for the 2.70 GeV/c data. The distributions have been fit with Legendre polynomials according to eq. 7. The fit results and the limits of the  $\Lambda$  cm momenta are given in each figure.

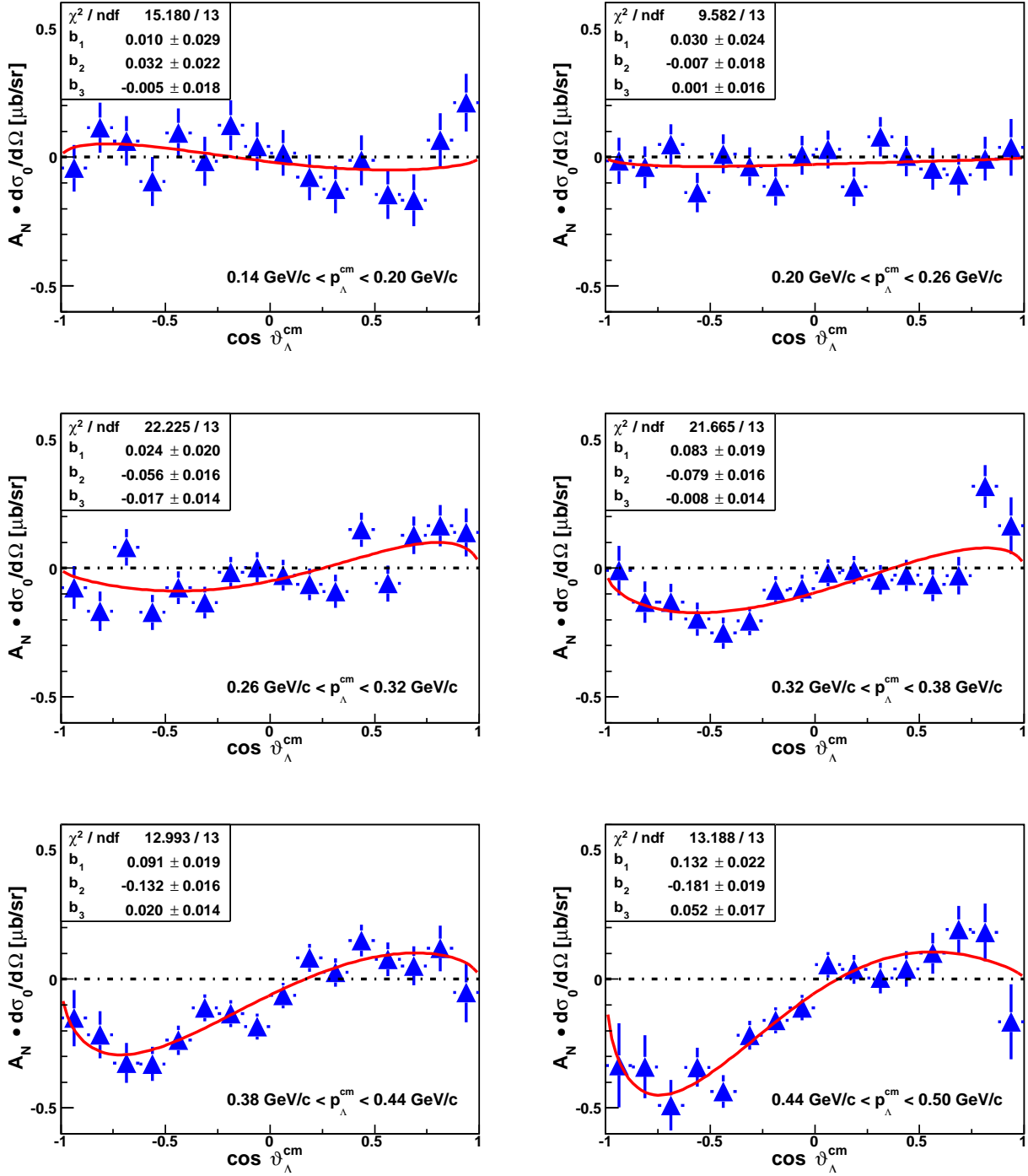


**Fig. 22.** The  $\Lambda$  analyzing power multiplied with the differential cross section is shown for different ranges of the  $\Lambda$  cm momentum for the 2.95 GeV/c data. The distributions have been fit with Legendre polynomials according to eq. 7. The fit results and the limits of the  $\Lambda$  cm momenta are given in each figure.

## 8 Appendix B

This appendix contains data tables with the measured quantities corresponding to figs. 2, 8, and 12.

**Table 4.**  $\Lambda$  polarization, dependence on  $\Lambda$  cm scattering angle

$\cos\vartheta_{\Lambda}^*$	$p_b = 2.70 \text{ GeV}/c$		$p_b = 2.95 \text{ GeV}/c$	
	polarization	$\pm$	polarization	$\pm$
-0.9375	-0.128	0.028	-0.023	0.026
-0.8125	-0.172	0.027	0.026	0.026
-0.6875	-0.130	0.026	0.060	0.026
-0.5625	-0.161	0.026	0.081	0.027
-0.4375	-0.184	0.026	0.098	0.028
-0.3125	-0.100	0.026	0.139	0.028
-0.1875	-0.142	0.026	0.131	0.029
-0.0625	-0.066	0.026	0.018	0.030
0.0625	-0.005	0.026	0.012	0.029
0.1875	0.021	0.026	-0.142	0.029
0.3125	0.124	0.026	-0.149	0.029
0.4375	0.051	0.025	-0.120	0.028
0.5625	0.183	0.025	-0.090	0.027
0.6875	0.227	0.025	-0.063	0.026
0.8125	0.220	0.026	-0.041	0.026
0.9375	0.167	0.028	0.039	0.028

**Table 5.**  $\Lambda$  polarization, dependence on Feynman  $x_F$ 

$x_F$	$p_b = 2.70 \text{ GeV}/c$		$p_b = 2.95 \text{ GeV}/c$	
	polarization	$\pm$	polarization	$\pm$
-0.9375	-0.340	0.166	0.153	0.147
-0.8125	-0.108	0.056	-0.019	0.053
-0.6875	-0.269	0.036	-0.010	0.035
-0.5625	-0.202	0.028	0.074	0.028
-0.4375	-0.180	0.023	0.063	0.024
-0.3125	-0.147	0.021	0.100	0.022
-0.1875	-0.076	0.020	0.073	0.021
-0.0625	-0.082	0.019	0.053	0.021
0.0625	-0.000	0.019	-0.029	0.021
0.1875	0.080	0.020	-0.101	0.022
0.3125	0.110	0.021	-0.131	0.023
0.4375	0.212	0.024	-0.084	0.025
0.5625	0.245	0.027	-0.044	0.029
0.6875	0.190	0.034	-0.054	0.036
0.8125	0.260	0.051	0.111	0.050
0.9375	0.621	0.121	0.211	0.115

**Table 6.**  $\Lambda$  polarization, dependence on the transversal momentum

$p_t \text{ [GeV}/c]$	$p_b = 2.70 \text{ GeV}/c$		$p_t \text{ [GeV}/c]$	$p_b = 2.95 \text{ GeV}/c$	
	polarization	$\pm$		polarization	$\pm$
0.016	-0.092	0.063	0.019	0.069	0.065
0.047	0.028	0.035	0.056	0.015	0.037
0.078	0.070	0.027	0.094	0.042	0.028
0.109	0.112	0.022	0.131	-0.038	0.023
0.141	0.086	0.019	0.169	-0.040	0.020
0.172	0.106	0.018	0.206	-0.036	0.019
0.203	0.127	0.018	0.244	-0.062	0.019
0.234	0.170	0.018	0.281	-0.077	0.020
0.266	0.166	0.020	0.319	-0.065	0.021
0.297	0.227	0.022	0.356	-0.166	0.024
0.328	0.161	0.027	0.394	-0.125	0.028
0.359	0.132	0.037	0.431	-0.206	0.035
0.391	0.008	0.102	0.469	-0.178	0.055
-	-	-	0.506	-0.281	0.165

**Table 7.** Analyzing power, 2.70 GeV/c data dependence on the cm scattering angle

$\cos(\vartheta^*)$	$A_N(\varphi^P)$	$\pm$	$A_N(\varphi^K)$	$\pm$	$A_N(\varphi^\Lambda)$	$\pm$
-0.9375	-0.002	0.014	0.080	0.019	-0.001	0.017
-0.8125	-0.003	0.014	0.131	0.018	-0.046	0.016
-0.6875	-0.018	0.015	0.177	0.017	-0.038	0.016
-0.5625	-0.055	0.016	0.155	0.017	-0.066	0.016
-0.4375	-0.055	0.016	0.181	0.016	-0.076	0.016
-0.3125	-0.046	0.017	0.141	0.016	-0.069	0.016
-0.1875	-0.085	0.017	0.151	0.016	-0.029	0.016
-0.0625	-0.076	0.018	0.156	0.016	-0.083	0.017
0.0625	-0.029	0.018	0.129	0.016	-0.045	0.016
0.1875	-0.007	0.018	0.107	0.016	-0.069	0.017
0.3125	-0.019	0.018	0.090	0.016	-0.047	0.017
0.4375	-0.071	0.018	0.071	0.016	-0.107	0.016
0.5625	-0.016	0.017	0.046	0.016	-0.107	0.016
0.6875	-0.056	0.016	0.016	0.016	-0.112	0.016
0.8125	-0.011	0.015	0.070	0.016	-0.065	0.016
0.9375	-0.023	0.016	0.052	0.017	-0.089	0.017

**Table 8.** Analyzing power, 2.95 GeV/c data dependence on the cm scattering angle

$\cos(\vartheta^*)$	$A_N(\varphi^P)$	$\pm$	$A_N(\varphi^K)$	$\pm$	$A_N(\varphi^\Lambda)$	$\pm$
-0.9375	0.015	0.016	0.071	0.024	-0.034	0.017
-0.8125	0.019	0.016	0.122	0.023	-0.065	0.017
-0.6875	0.013	0.018	0.171	0.020	-0.057	0.017
-0.5625	-0.052	0.018	0.189	0.019	-0.129	0.018
-0.4375	-0.088	0.019	0.188	0.018	-0.119	0.019
-0.3125	-0.084	0.019	0.135	0.018	-0.100	0.019
-0.1875	-0.022	0.019	0.150	0.018	-0.057	0.020
-0.0625	-0.095	0.019	0.189	0.018	-0.048	0.020
0.0625	-0.078	0.020	0.149	0.018	-0.020	0.019
0.1875	-0.089	0.020	0.089	0.018	-0.015	0.020
0.3125	-0.075	0.020	0.060	0.018	-0.011	0.019
0.4375	-0.087	0.020	0.070	0.018	0.048	0.019
0.5625	-0.002	0.020	-0.003	0.018	0.001	0.019
0.6875	0.005	0.019	-0.003	0.018	0.009	0.018
0.8125	0.041	0.018	-0.035	0.018	0.066	0.017
0.9375	0.058	0.019	-0.000	0.022	0.027	0.018



**Table 9.** Analyzing power, 2.70 GeV/c data dependence on Feynman  $x_F$ 

$x_F$	$A_N(\varphi^P)$	$\pm$	$A_N(\varphi^K)$	$\pm$	$A_N(\varphi^\Lambda)$	$\pm$
-0.9375	-0.014	0.056	0.144	0.081	0.110	0.096
-0.8125	-0.002	0.024	0.118	0.033	0.043	0.034
-0.6875	-0.018	0.017	0.207	0.022	-0.000	0.022
-0.5625	-0.051	0.015	0.181	0.017	-0.056	0.017
-0.4375	-0.016	0.014	0.133	0.015	-0.056	0.015
-0.3125	-0.026	0.013	0.144	0.014	-0.069	0.013
-0.1875	-0.062	0.013	0.143	0.013	-0.047	0.012
-0.0625	-0.057	0.013	0.136	0.013	-0.065	0.012
0.0625	-0.024	0.013	0.119	0.013	-0.062	0.012
0.1875	-0.030	0.014	0.110	0.013	-0.057	0.013
0.3125	-0.042	0.015	0.077	0.014	-0.089	0.014
0.4375	-0.051	0.015	0.042	0.014	-0.085	0.015
0.5625	-0.031	0.017	0.044	0.015	-0.141	0.017
0.6875	-0.011	0.020	0.031	0.018	-0.067	0.021
0.8125	0.031	0.027	0.023	0.026	-0.093	0.031
0.9375	-0.005	0.068	-0.041	0.071	-0.090	0.073

**Table 10.** Analyzing power, 2.95 GeV/c data dependence on Feynman  $x_F$ 

$x_F$	$A_N(\varphi^P)$	$\pm$	$A_N(\varphi^K)$	$\pm$	$A_N(\varphi^\Lambda)$	$\pm$
-0.9375	0.030	0.064	-0.091	0.123	-0.311	0.093
-0.8125	0.007	0.026	0.185	0.050	-0.105	0.035
-0.6875	0.021	0.019	0.134	0.028	-0.043	0.023
-0.5625	-0.009	0.017	0.155	0.020	-0.108	0.019
-0.4375	-0.044	0.016	0.164	0.017	-0.112	0.016
-0.3125	-0.054	0.015	0.175	0.015	-0.089	0.015
-0.1875	-0.043	0.015	0.130	0.014	-0.066	0.014
-0.0625	-0.051	0.015	0.173	0.014	-0.029	0.014
0.0625	-0.067	0.015	0.157	0.014	-0.023	0.014
0.1875	-0.105	0.016	0.073	0.015	-0.000	0.015
0.3125	-0.025	0.017	0.070	0.015	0.009	0.016
0.4375	0.004	0.018	0.007	0.016	0.036	0.017
0.5625	0.035	0.020	-0.042	0.018	0.076	0.019
0.6875	0.019	0.022	-0.064	0.021	0.076	0.024
0.8125	0.073	0.029	-0.144	0.031	-0.055	0.033
0.9375	0.122	0.063	0.032	0.079	0.080	0.075

**Table 11.** Analyzing power, 2.70 GeV/c data dependence on transversal momentum

$p_t$ [GeV/c]	$A_N(\varphi^p)$	$\pm$	$A_N(\varphi^K)$	$\pm$	$A_N(\varphi^\Lambda)$	$\pm$
0.016	0.071	0.108	0.143	0.048	-0.064	0.038
0.047	-0.008	0.022	0.030	0.020	-0.069	0.022
0.078	-0.016	0.014	0.067	0.015	-0.029	0.017
0.109	-0.028	0.012	0.087	0.013	-0.032	0.014
0.141	0.002	0.011	0.113	0.012	-0.064	0.012
0.172	-0.035	0.011	0.116	0.011	-0.073	0.011
0.203	-0.035	0.011	0.110	0.011	-0.066	0.011
0.234	-0.038	0.012	0.142	0.011	-0.088	0.011
0.266	-0.049	0.013	0.114	0.011	-0.086	0.012
0.297	-0.056	0.016	0.117	0.013	-0.057	0.014
0.328	-0.086	0.020	0.122	0.042	-0.080	0.017
0.359	-0.113	0.027	-	-	-0.039	0.023
0.391	-0.115	0.117	-	-	-0.045	0.064

**Table 12.** Analyzing power, 2.95 GeV/c data dependence on transversal momentum

$p_t$ [GeV/c]	$A_N(\varphi^p)$	$\pm$	$A_N(\varphi^K)$	$\pm$	$A_N(\varphi^\Lambda)$	$\pm$
0.019	0.111	0.113	0.094	0.061	-0.014	0.041
0.056	-0.057	0.032	0.019	0.027	0.033	0.024
0.094	0.023	0.020	0.066	0.020	0.017	0.018
0.131	0.002	0.016	0.112	0.017	-0.009	0.015
0.169	0.026	0.014	0.117	0.015	-0.015	0.014
0.206	0.002	0.014	0.129	0.013	0.001	0.013
0.244	0.020	0.014	0.114	0.012	-0.018	0.013
0.281	0.002	0.014	0.091	0.012	-0.048	0.013
0.319	-0.039	0.014	0.085	0.012	-0.081	0.014
0.356	-0.066	0.015	0.080	0.015	-0.059	0.016
0.394	-0.111	0.016	0.067	0.019	-0.073	0.019
0.431	-0.169	0.019	0.131	0.048	-0.089	0.024
0.469	-0.128	0.026	-	-	-0.103	0.037
0.506	-0.148	0.084	-	-	-0.221	0.110

**Table 13.**  $D_{NN}$ , dependence on  $\Lambda$  cm scattering angle

$\cos\vartheta_{\Lambda}^*$	$p_b = 2.70 \text{ GeV}/c$		$p_b = 2.95 \text{ GeV}/c$	
	$D_{NN}$	$\pm$	$D_{NN}$	$\pm$
-0.9375	-0.645	0.070	-0.172	0.070
-0.8125	-0.384	0.067	-0.179	0.070
-0.6875	-0.523	0.066	-0.263	0.072
-0.5625	-0.473	0.065	-0.453	0.074
-0.4375	-0.347	0.065	-0.435	0.076
-0.3125	-0.445	0.065	-0.485	0.077
-0.1875	-0.365	0.066	-0.275	0.080
-0.0625	-0.226	0.067	-0.260	0.080
0.0625	-0.305	0.066	-0.318	0.079
0.1875	-0.321	0.066	-0.182	0.080
0.3125	-0.215	0.066	-0.383	0.078
0.4375	-0.315	0.064	-0.323	0.076
0.5625	-0.430	0.064	-0.252	0.075
0.6875	-0.349	0.065	-0.420	0.071
0.8125	-0.455	0.065	-0.407	0.070
0.9375	-0.498	0.072	-0.256	0.075

**Table 14.**  $D_{NN}$ , dependence on Feynman  $x_F$ 

$x_F$	$p_b = 2.70 \text{ GeV}/c$		$p_b = 2.95 \text{ GeV}/c$	
	$D_{NN}$	$\pm$	$D_{NN}$	$\pm$
-0.9375	0.181	0.422	0.206	0.401
-0.8125	-0.636	0.140	0.042	0.144
-0.6875	-0.306	0.091	0.040	0.096
-0.5625	-0.407	0.070	-0.268	0.076
-0.4375	-0.497	0.059	-0.284	0.066
-0.3125	-0.447	0.054	-0.313	0.061
-0.1875	-0.469	0.050	-0.559	0.058
-0.0625	-0.333	0.049	-0.305	0.057
0.0625	-0.349	0.049	-0.259	0.057
0.1875	-0.235	0.050	-0.323	0.059
0.3125	-0.306	0.054	-0.243	0.062
0.4375	-0.517	0.060	-0.391	0.068
0.5625	-0.379	0.069	-0.410	0.078
0.6875	-0.530	0.086	-0.355	0.096
0.8125	-0.348	0.128	-0.426	0.134
0.9375	-0.285	0.312	-0.452	0.313

**Table 15.**  $D_{NN}$ , dependence on the transversal momentum

$p_t \text{ [GeV}/c]$	$p_b = 2.70 \text{ GeV}/c$		$p_t \text{ [GeV}/c]$	$p_b = 2.95 \text{ GeV}/c$	
	$D_{NN}$	$\pm$		$D_{NN}$	$\pm$
0.016	-0.784	0.157	0.019	-0.231	0.172
0.047	-0.707	0.089	0.056	-0.217	0.098
0.078	-0.505	0.068	0.094	-0.408	0.075
0.109	-0.503	0.056	0.131	-0.338	0.061
0.141	-0.438	0.048	0.169	-0.298	0.055
0.172	-0.460	0.045	0.206	-0.350	0.053
0.203	-0.319	0.045	0.244	-0.337	0.052
0.234	-0.370	0.046	0.281	-0.292	0.054
0.266	-0.457	0.050	0.319	-0.366	0.058
0.297	-0.266	0.056	0.356	-0.294	0.064
0.328	-0.034	0.067	0.394	-0.246	0.076
0.359	-0.160	0.094	0.431	-0.253	0.096
0.391	0.034	0.258	0.469	-0.244	0.150
-	-	-	0.506	0.000	0.456

## References

1. S. Jowzaee et al. (COSY-TOF), Eur. Phys. J. **A52**, 7 (2016)
2. G. Bunce et al., Phys. Rev. Lett. **36**, 1113 (1976)
3. T.A. DeGrand, H.I. Miettinen, Phys. Rev. **D24**, 2419 (1981)
4. G. Agakishiev et al. (HADES), Eur. Phys. J. **A50**, 81 (2014)
5. S. Choi (DISTO), Nucl. Phys. **A639**, 1 (1998)
6. R. Muenzer, *private communications* (2015)
7. B.E. Bonner et al., Phys. Rev. Lett. **58**, 447 (1987)
8. B.E. Bonner et al., Phys. Rev. **D38**, 729 (1988)
9. A. Bravar et al. (E704), Phys. Rev. Lett. **78**, 4003 (1997)
10. F. Balestra et al. (DISTO), Phys. Rev. Lett. **83**, 1534 (1999)
11. F. Hauenstein, Ph.D. thesis, University Erlangen-Nuernberg (2014), <http://opus4.kobv.de/opus4-fau/frontdoor/index/index/docId/5614>
12. S. Jowzaee, Ph.D. thesis, Jagiellonian University Cracow (2014), <http://juser.fz-juelich.de/record/185801>
13. R. Arndt, W. Briscoe, I. Strakovsky, R. Workman, Phys. Rev. **C76**, 025209 (2007)
14. M. Röder et al. (COSY-TOF), Eur. Phys. J. **A49**, 157 (2013)
15. R. Gebel, O. Felden, R. Maier, AIP Conf.Proc. **980**, 231 (2008)
16. D. Besset et al., Nucl. Instrum. Meth. **166**, 515 (1979)
17. G.G. Ohlsen, P.W. Keaton, Nucl. Instrum. Meth. **109**, 41 (1973)
18. K. Olive et al. (Particle Data Group), Chin.Phys. **C38**, 090001 (2014)
19. K.J. Heller et al., Phys. Rev. Lett. **41**, 607 (1978)
20. F. Abe et al., Phys. Rev. **D34**, 1950 (1986)
21. A.M. Smith et al. (R608), Phys. Lett. **B185**, 209 (1987)
22. J. Felix et al., Phys. Rev. Lett. **76**, 22 (1996)
23. J. Felix et al., Phys. Rev. Lett. **82**, 5213 (1999)
24. B. Lundberg et al., Phys. Rev. **D40**, 3557 (1989)
25. J. Felix et al. (E690), Phys. Rev. Lett. **88**, 061801 (2002)
26. E. Ramberg et al., Phys. Lett. **B338**, 403 (1994)
27. V. Fanti et al. (NA48), Eur. Phys. J. **C6**, 265 (1999)
28. I. Abt et al. (HERA-B), Phys. Lett. **B638**, 415 (2006)
29. G. Aad et al. (ATLAS), Phys. Rev. **D91**(3), 032004 (2015)
30. H.A. Neal, E. De La Cruz Burelo (2006), [arXiv: hep-ph/0602079](https://arxiv.org/abs/hep-ph/0602079)
31. E.C. Dukes et al., Phys. Lett. **B193**, 135 (1987)
32. T. Henkes et al. (R608), Phys. Lett. **B283**, 155 (1992)
33. J. Felix, AIP Conf. Proc. **857B**, 320 (2006)
34. J. Felix et al., PoS **HEP2005**, 122 (2006)
35. M. Maggiora (DISTO), Nucl. Phys. **A691**, 329 (2001)
36. F. Balestra (DISTO), Nucl. Phys. Proc. Suppl. **93**, 58 (2001)
37. A. Saha et al., Phys. Rev. Lett. **51**, 759 (1983)
38. J.A. Niskanen, AIP Conf. Proc. **69**, 62 (1981)
39. A. Gasparyan, J. Haidenbauer, C. Hanhart, Phys. Rev. **C72**, 034006 (2005)
40. F. Hauenstein et al. (COSY-TOF) (2016), [arXiv: nuc1-ex/1607.04783](https://arxiv.org/abs/nuc1-ex/1607.04783)
41. F. Hauenstein et al., Nucl. Instrum. Meth. **A817**, 42 (2016)
42. A. Lesnik et al., Phys. Rev. Lett. **35**, 770 (1975)
43. F. Balestra et al. (DISTO), Nucl. Instrum. Meth. **A426**, 385 (1999)
44. J. Laget, Phys. Lett. **B259**, 24 (1991)
45. G. Fäldt, C. Wilkin, Eur. Phys. J. **A24**, 431 (2005)